

Orbital interactions and chemical reactivity of metal particles and metal surfaces

Citation for published version (APA):

Santen, van, R. A., & Baerends, E. J. (1991). Orbital interactions and chemical reactivity of metal particles and metal surfaces. In Z. B. Maksic (Ed.), *Theoretical treatment of large molecules and their interactions* (pp. 323-389). (Theoretical models of chemical bonding; Vol. 4). Springer.

Document status and date:

Published: 01/01/1991

Document Version:

Publisher's PDF, also known as Version of Record (includes final page, issue and volume numbers)

Please check the document version of this publication:

- A submitted manuscript is the version of the article upon submission and before peer-review. There can be important differences between the submitted version and the official published version of record. People interested in the research are advised to contact the author for the final version of the publication, or visit the DOI to the publisher's website.
- The final author version and the galley proof are versions of the publication after peer review.
- The final published version features the final layout of the paper including the volume, issue and page numbers.

[Link to publication](#)

General rights

Copyright and moral rights for the publications made accessible in the public portal are retained by the authors and/or other copyright owners and it is a condition of accessing publications that users recognise and abide by the legal requirements associated with these rights.

- Users may download and print one copy of any publication from the public portal for the purpose of private study or research.
- You may not further distribute the material or use it for any profit-making activity or commercial gain
- You may freely distribute the URL identifying the publication in the public portal.

If the publication is distributed under the terms of Article 25fa of the Dutch Copyright Act, indicated by the "Taverne" license above, please follow below link for the End User Agreement:

www.tue.nl/taverne

Take down policy

If you believe that this document breaches copyright please contact us at:

openaccess@tue.nl

providing details and we will investigate your claim.

Orbital Interactions and Chemical Reactivity of Metal Particles and Metal Surfaces

R. A. van Santen

E. J. Baerends

Laboratory of Inorganic Chemistry and Catalysis, Technical University of Eindhoven, P.O. Box 513,
5600 MB Eindhoven, The Netherlands

Department of Theoretical Chemistry, Free University Amsterdam, De Boelelaan 7161, 1007 MC
Amsterdam

This review of chemical bonding to metal surfaces and small metal particles demonstrates the power of symmetry concepts to predict changes in chemical bonding.

Ab-initio-calculations of chemisorption to small particles, as well as semiempirical extended Hückel calculations applied to the study of the reactivity of metal slabs are reviewed.

On small metal particles, classical notions of electron promotion and hybridization are found to apply. The surroundings of a metal atom (ligands in complexes, other metal atoms at surfaces), affect bonding and reactivity through the prehybridization they induce. A factor specific for large particles and surfaces is the required localization of electrons on the atoms involved in the metal surface bond.

At the surface, the bondenergy is found to relate to the grouporbital local density of states at the Fermi level. The use of this concept is extensively discussed and illustrated for chemisorption of CO and dissociation of NO on metal surfaces.

A discussion is given of the current decomposition schemes of bond energies and related concepts (exchange (Pauli-)repulsion, polarization, charge transfer). The role of non-orthogonality of fragment orbitals and of kinetic and potential energy for Pauli repulsion and (orbital)polarization is analyzed.

Numerous examples are discussed to demonstrate the impact of those concepts on chemical bonding theory.

1 Introduction	324
2 Theoretical Intermezzo	328
2.1 Analysis of Bonding Energies	329
2.2 The Extended Hückel Method	338
2.3 The Effect of Overlap on the Bond Energy According to the Extended Hückel Method	339
2.4 Embedded Systems	346
3 Bonding to Metal Clusters	358
3.1 Chemisorption and Dissociation (Oxidative Addition) of H ₂ to Transition Metal Atoms	358
3.2 Reaction of H ₂ with Transition Metal Clusters	365
3.3 Cluster Chemisorption Models of CO Adsorption	372
4 Chemisorption to Metal Surfaces	377
5 Summary	386
6 List of Symbols	386
7 References	387

1 Introduction

The increased interest for surfaces and interphases within the past decade has also led to a considerable extension of the quantum chemist's sphere of interest.

Extensive ab-initio calculations have been done on small metal clusters simulating adsorption sites on surfaces. Semiempirical extended Hückel calculations have been applied to study the reactivity of metal slabs and also the techniques of the solid state physicist with the aim to calculate from first principles the interaction between adsorbing molecules and metal surfaces.

As a result, our understanding of the relation between structure and chemical bonding, especially of bonds between metal atoms and adsorbates, has considerably improved.

In this review we will discuss the current state of knowledge in relation to the "classical" frontier orbital concept in terms of interactions between highest occupied molecular orbitals (HOMO) and lowest unoccupied molecular orbitals (LUMO) [1, 2, 3].

If a molecule approaches a metal surface and is at a distance from the surface which is large compared to the spatial extension of the electron distribution around the atoms, some attraction will be experienced due to induction and van der Waals interactions.

The theory of van der Waals interactions in small atom clusters is well established [4] and has recently also been reviewed for the interaction with metal surfaces [5]. The attractive van der Waals interaction with a metal surface can be considered to be due to the image potentials generated on the metal surface by the fluctuating charge distributions of the interacting molecule.

As long as interaction is weak, the electrons in a metal rapidly adjust to the motions of the electrons in a molecule [6].

Induction forces are generated by the interaction of the induced image potential with the stationary multipoles of the charge distribution of the molecule in the ground state.

Though these contributions to the surface bond will not be considered in this review, one should note that these terms may become important when interactions are weak. They may be of relevance for so-called "precursor" states that are short-lived and are observed in surface molecular beam experiments [7] or postulated in thermal desorption experiments [8].

The Hartree-Fock approximation on which most of our considerations will be based does not include those effects.

Electrostatic long-range forces between metal surfaces and a molecule at a large distance may exist if the surface has become nonhomogeneous, because of the presence of atoms with different configurations (steps or kinks). This is the case for higher Miller index surfaces or if other molecules or atoms have been adsorbed to the surface. Localized dipoles may then exist, leading to long-range Coulombic interactions. The existence of such potentials has been experimentally demonstrated by Geerlings and Los [9] for Li adsorbed on W and has been theoretically calculated for K on Pt [10, 11].

Chemical bonding is considerably affected by the presence of such electrostatic potentials, because the relative position of the adsorbing molecule's molecular orbital

energy levels with respect to the metal-surface Fermi level is changed as will be discussed later.

The next terms to consider arise if the atom distances become so small that charge transfer between adsorbate and metal surface becomes possible. The energy cost involved is compensated for by the electrostatic interaction between separated charges in small clusters or by the image potential induced in a metal by the charge on the adsorbing molecule. Distances may still be large compared to the spatial extension of the electron distributions between the atoms. The resulting negative ions sometimes are short-lived and are only observed in molecular beam experiments or at low temperatures. For molecules, these weakly bonded states can be considered to be the precursor states [7, 8] for dissociation. A well-known example is the negative ion of molecular oxygen found at low temperatures at single crystal silver surfaces [12, 13].

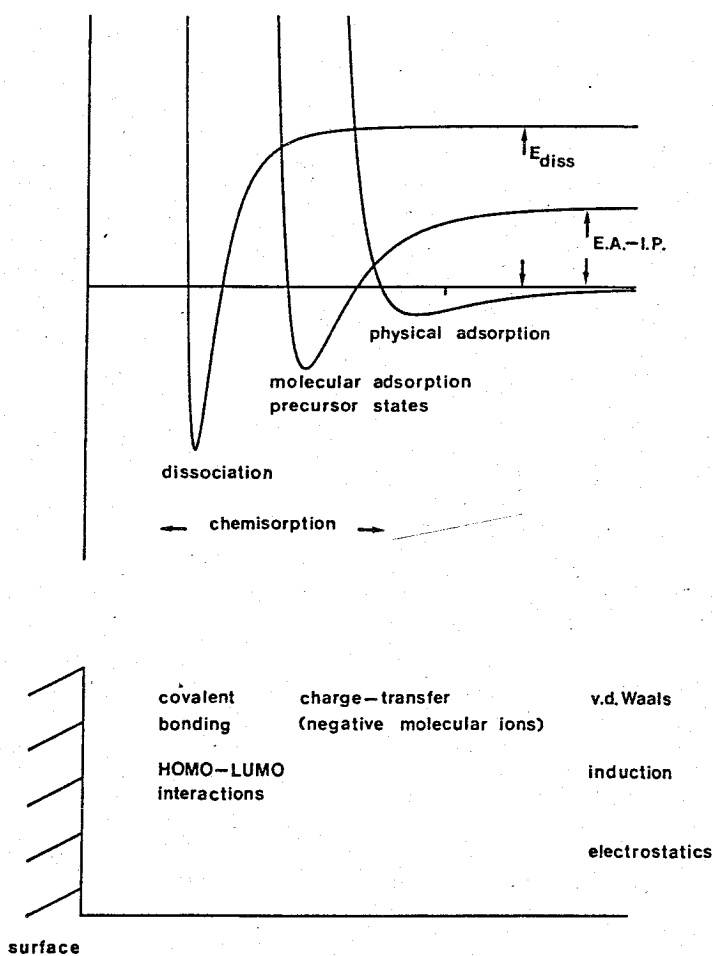


Fig. 1. Types of interaction energies and potential-energy diagram of a molecule approaching a surface [14]

Alkali atoms become positively charged and are strongly chemisorbed to the metal surface by a potential dominated by the alkali ion-induced image potential.

In this review we will not discuss the interaction regimes mentioned so far, but rather focus on the chemical bonding effects that occur if the distances become short enough for the electron distributions to overlap. The successive stages of interaction are schematically sketched in Fig. 1.

In the past decade considerable attention has been paid to an analysis of chemical bonding in physically meaningful contributions such as steric repulsion, electrostatic attraction/repulsion, charge transfer, polarization, etc. We may refer to the work by Morokuma et al. [15, 16, 17], Whangbo et al. [18], Bernardi, Bottoni et al. [19] and Stone and Erskine [20]. Applications of such analyses to transition-metal complexes have been carried out by Morokuma et al. [21], Ziegler [22, 23], Bauschlicher and Bagus [24], and Baerends and Rozendaal [25].

Applications to adsorbates interacting with small clusters of metal atoms are found in the work of Post and Baerends [26] and Bagus et al. [27, 28, 29].

These analyses have considerably enhanced our understanding of the main factors governing metal-ligand (or surface-adsorbate) interactions but they sometimes lead to misunderstanding and are not even without ambiguity.

In the next section, the basic features of decomposition schemes for bond energies will be discussed. In particular, we wish to stress the importance of other interactions than the charge-transfer type HOMO-LUMO interactions commonly employed in frontier orbital considerations. Important contributions arise also from polarization of the interacting units, especially in the highly polarizable metallic substrates, and from repulsive interaction with occupied (sub-)valence shells contributing to the steric repulsion. The latter interaction in fact determines the bond distances as it is responsible for the inner, repulsive, part of the potential energy curves.

The physical origin of the repulsion is the Pauli exclusion principle which forbids the presence of two electrons with the same spin at the same position. As will be shown, this leads to a depletion of charge in the overlap region, which is associated with a strong rise in kinetic energy that is only partly cancelled by a more favorable potential energy.

We will discuss in some detail how and to what extent these effects are described in the simple extended Hückel approximation.

As will be demonstrated, the incorporation of the overlap between the interacting fragment orbitals plays a key role in the extended Hückel analysis, in keeping with the picture sketched above.

If two orbitals interact, the average position of the levels after the interaction will be shifted upwards by an amount roughly proportional to the overlap and to the Hamiltonian interaction matrix elements (transfer integrals, overlap-energy integrals). If the two orbitals are fully occupied, this leads to the well-known 4-electron destabilizing interaction (compare He_2), as nicely illustrated by a calculation of Bagus et al. [30], Fig. 2. Such repulsive interactions always occur between the occupied orbitals of the interacting units. At the surface they are especially important because they will strongly compete with the differences in attractive energy between topologically different sites [3]. This has consequences for reactivity since the way a molecule adsorbs to a metal surface may affect its subsequent reaction mode.

A similar role of changes in kinetic energy is found if the metal is simulated by a

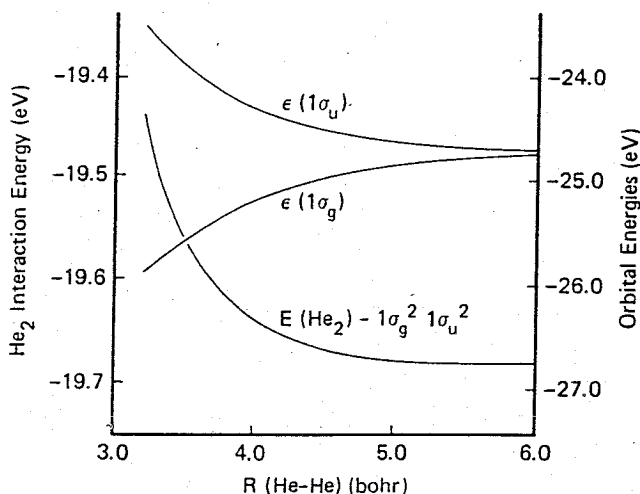


Fig. 2. SCF potential curve for He_2 ; the interaction energy is shown on the left-hand scale; the orbital energies, $E(1\sigma_g)$ and $E(1\sigma_u)$, as a function of He—He distance, R_0 (He—He); the latter values are shown in the right-hand scale [30]

free electron gas as discussed by Norskov [31] and illustrated in Fig. 3. In the case of chemisorption of atoms, the first-order term to chemical bonding is determined by the change in electron density of the adsorbing atom embedded in the metal surface. To a good approximation, bonding occurs because the atom electron density is replaced by the density of the metal surface. If the atom density is low, an increase in bonding is observed because the negative charge on the embedded atom resulting from the higher metal electron density is stabilized by screening of this charge by the surrounding jellium. This is the earlier discussed induced image potential stabilization of charged adsorbate states. However, if the electron density of the jellium increases,

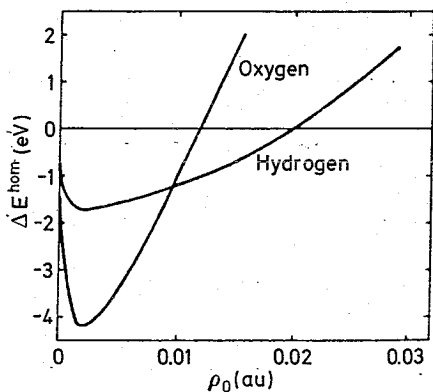


Fig. 3. Energy ΔE^{hom} of hydrogen and oxygen embedded in infinite jellium as a function of jellium density ρ_0 . The energy zero is the energy of the free atom [16]

the resulting interaction becomes repulsive. A high density on the embedded atom becomes unfavorable because according to free electron theory, the repulsive kinetic energy increases faster with density than the intraatomic exchange energy.

A second topic that will be highlighted in this review is the role of the immediate neighborhood of the metal atom(s) that interact with an incoming ligand (adsorbate): the ancillary ligands in a mononuclear complex (cf. homogeneous catalysis) and the surrounding metal atoms in a semi-infinite lattice (heterogeneous catalysis).

Attractive interactions require hybridization of available orbitals so as to optimize overlap between interacting orbitals. Similar to the Pauling hybridization concept [32], promotion energy is required to redistribute the electrons from the ground state to the state giving the largest amount of bonding. This will be illustrated in Sect. 3 for bonding to isolated transition-metal atoms.

There is an important difference between bonding to single metal atoms, metal atoms surrounded by ligands, and atoms embedded in a metal surface. Bonding to ligands forces the electrons of a metal atom often into a particular mode of hybridization which directs orbitals to a vacant position such that bonding is optimized with a reacting fragment. In such a case little promotion energy may be required.

The metal neighbors of a metal surface atom will have a similar effect on hybridization as the ligands in the organometallic complex [33]. In Sect. 4 we will focus on a special additional feature of the interaction with metal surfaces, namely the energy cost involved due to delocalized electrons [33–37]. In order to bind an electron participating in the chemisorptive bond, it has to decouple from the bonds with the other metal atoms. This localization energy often decreases the bond strength in a complex with respect to that in a free molecule. It also results in weaker bonds between the metal surface atoms after the chemisorptive bond has been formed.

Bonding to a metal surface can also be described in terms of frontier orbital interactions similar as in the cluster case. Symmetry considerations now apply to the coefficients of the metalsurface molecular orbitals at the Fermi levels that interact with the HOMOs and LUMOs of the adsorbing molecule or atom. Such a theory helps to predict bonding topology of adsorbates, as will be illustrated for bonding of CO to the transition metals.

It will also be used to predict differences in reactivity of transition metal surfaces.

In the last section, differences in reactivity of transition metal surfaces as compared to clusters will be highlighted.

2 Theoretical Intermezzo

In the following, we will describe the theoretical basis for the quantum chemical expressions used for the analysis of metal-ligand interactions described in later sections.

First, the various decomposition schemes of the interaction energy that are currently used will be briefly reviewed with emphasis on the differences. The role of the potential energy and kinetic energy in the steric repulsion will be delineated, as well as the different ways to treat the frontier orbital interaction, i.e., charge-transfer and polarization type of orbital mixings.

The role of overlap in Pauli repulsion will be stressed. The extended Hückel method will be applied to clusters as well as semi-infinite systems.

Then the relevant theoretical concepts to be used in bonding to semi-infinite systems with a continuous distribution of energy levels, instead of discrete levels as in clusters, will be introduced.

2.1 Analysis of Bonding Energies

Let us consider the interaction between two systems A and B with wave functions Ψ_A and Ψ_B , resp., and energies E_A and E_B , resp.

Although analysis of the bonding energy is not only possible for one-determinantal wave functions, it is most simply carried out and illustrated using such wave functions. We thus take:

$$\Psi_A = |\varphi_1 \dots \varphi_a|, \quad \Psi_B = |\phi_1 \dots \phi_b|$$

where φ_1 to φ_a are the one-electron wave functions of fragment A, and ϕ_1 to ϕ_b are the one-electron wave functions of fragments B. The vertical bars denote antisymmetrization as well as normalization.

As the first step in the bonding process, we consider the wave function Ψ^0 which consists of just the product $\Psi_A \Psi_B$, suitably antisymmetrized and normalized:

$$\Psi^0 = N \hat{A} \{ \Psi_A \Psi_B \} = |\varphi_1 \dots \varphi_a \phi_1 \dots \phi_b| \quad (1)$$

The total energy is then given by the expression:

$$E^0 = \langle \Psi^0 | H | \Psi^0 \rangle,$$

and the bond strength becomes:

$$\Delta E^0 = E^0 - E_A - E_B$$

The energy ΔE^0 computed within this approximation is in general positive (repulsive). It is important to realize that this is not due to electrostatic (Coulomb) interactions between the electrons and nuclei of A with those of B. The electrostatic interaction energy

$$\begin{aligned} \Delta E_{\text{elstat}} = & \int \varrho^A(1) \varrho^B(2) / r_{12} \, d\vec{r}_1 \, d\vec{r}_2 + \sum_{\alpha \in A} \sum_{\beta \in B} Z_\alpha Z_\beta / R_{\alpha\beta} \\ & + \int V_N^A(1) \varrho^B(1) \, d\vec{r}_1 + \int V_N^B(1) \varrho^A(1) \, d\vec{r}_1 \end{aligned}$$

where $V_N^A(V_N^B)$ is the nuclear potential of fragment A (resp. B) and $Z_\alpha(Z_\beta)$ are the nuclear charges of A (resp. B), is for neutral systems negative (attractive), except at very short distances. This is simply verified for two atoms with spherically symmetrical charge distributions ϱ^A and ϱ^B , where it is seen to arise from the overlap of the diffuse charge distributions (for instance, the repulsion between ϱ^A and ϱ^B is less than the one between Z_A and Z_B).

What is the origin of the repulsive character of E^0 , given that it is not a simple charge superposition effect? Let us first note that the charge distribution corresponding to Ψ^0 is not simply the sum of q^A and q^B . We have to evaluate the electron density taking the non-orthogonality into account, or alternatively we have to orthogonalize the $\{\phi_i\}$ and $\{\phi_j\}$ sets (Schmidt, Löwdin or otherwise), which does not change the wave function, but which allows us to write the electron density as the familiar sum of orbital densities.

The density q^0 differs from $q_A + q_B$ in that charge is removed from the overlap region.

Consider the case of one orbital ϕ_A on A, and ϕ_B on B, with $S = \langle \phi_A | \phi_B \rangle$. One finds for the antisymmetrized and normalized product function:

$$\Psi^0(1,2) = N \hat{A} \{ \phi_A(1) \phi_B(2) \} = \frac{1}{\sqrt{2-2S^2}} \{ \phi_A(1) \phi_B(2) - \phi_A(2) \phi_B(1) \}$$

with a corresponding one-electron density distribution:

$$\begin{aligned} q^0(1) &= 2 \int |\psi^0(1,2)|^2 d\vec{r}_2 \\ &= \frac{1}{1-S^2} \{ |\phi_A(1)|^2 + |\phi_B(1)|^2 - 2S\phi_A(1)\phi_B(1) \} \end{aligned} \quad (2)$$

Expression $q^0(1)$ gives the one-electron distribution of two fragments with overlapping orbitals, without any covalent or other bonding effects present. The changed density $q^0(1)$ is only the result of conservation of charge and the Pauli exclusion principle.

Exactly the same expression results if one orthogonalizes ϕ_B on ϕ_A to give $\phi'_B = (1-S^2)^{-1/2}(\phi_B - S\phi_A)$ (Schmidt orthogonalization) which allows to write Ψ^0 as a determinantal wave function with orthogonal orbitals: $\Psi^0(1,2) = |\phi_A(1)\phi'_B(2)|$ and $q^0(1) = |\phi_A|^2 + |\phi'_B|^2$.

It is clear from Eq. (2) that the overlap term in q^0 causes depletion of charge in the overlap region. This is demonstrated in Fig. 4, with a contour plot of $\Delta q^0 = q^0 - q_A - q_B$ for the $K^+ - W$ system [38].

The density change Δq^0 results in changes in both the potential and the kinetic energy. As for the potential energy, the already negative ΔE_{elstat} is changed into an even more negative (attractive) total potential energy as electron density moves to regions closer to the highly attractive nuclei.

It is in fact well known from Ruedenberg's analysis of the chemical bond [39] that building up of a bond density that is usually associated with bond formation is not favorable from a potential energy point of view, but has to be judged against the favorable decrease of kinetic energy associated with a more slowly varying density in the internuclear region, and the unfavorable increase in kinetic energy associated with piling up electron density in the region of low potential energy close to the nucleus.

In keeping with this analysis, it is the latter effect, the rise in kinetic energy, which is the origin of the repulsive character of ΔE^0 . This is illustrated by the kinetic and potential energy contributions to ΔE^0 of $K^+ - W$ given in Table 1.

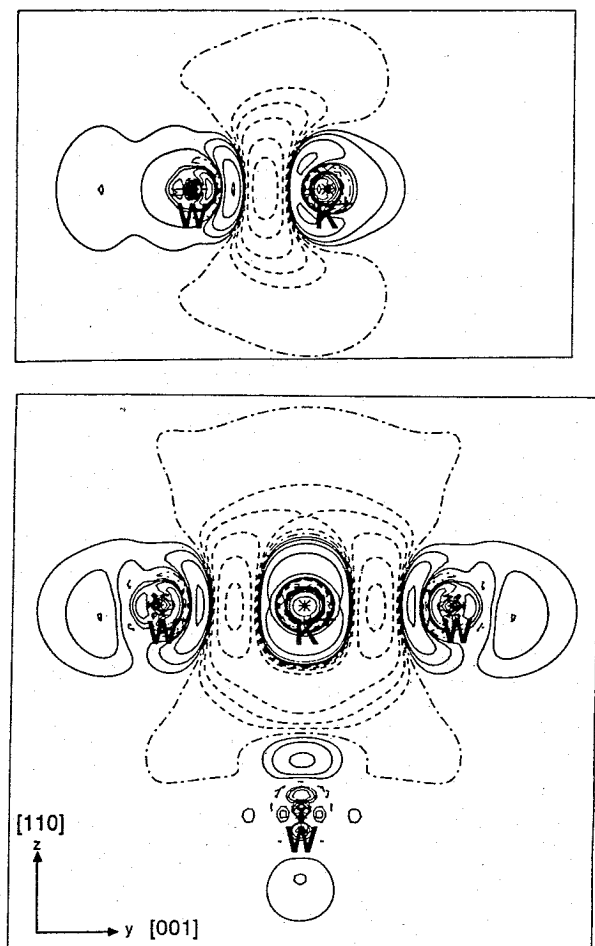


Fig. 4. Contourplot of the change $\Delta\rho^0$ in electron charge density due to the $K^+ - W$ ion-atom (see text). Solid contours indicate $\Delta\rho^0 > 0$, dashed contours $\Delta\rho^0 < 0$, and dot-dashed contours $\Delta\rho^0 = 0$. Contours drawn are $\Delta\rho^0 = 0, \pm .005, \pm 1.01, \pm 0.02, \pm 0.05, \pm 0.1, \pm 0.2$, and $\pm 0.5 e/a_0^3$ [38]

It is possible to qualitatively understand the increase in kinetic energy due to the density change $\Delta\rho^0$ from the relation between the kinetic energy and the gradient of an orbital $\nabla\psi$, and of the orbital density $\nabla\rho = \psi^*(\nabla\psi) + (\nabla\psi^*)\psi$:

$$E_{\text{kin}} = -\frac{1}{2} \int \psi^* \nabla^2 \psi \, d\tau = \frac{1}{2} \int |\nabla\psi|^2 \, d\tau$$

ΔE^0 is denoted in various ways in the literature. If the electrostatic contribution to ΔE^0 is separated, the remainder is commonly referred to as exchange (or Pauli-) repulsion (Fujimoto [40], Morokuma [15]) to indicate that this effect derives from the anti-symmetry requirement on the wave function:

$$\Delta E^0 = \Delta E_{\text{elstat}} + \Delta E_{\text{XREP}} \quad (3)$$

Table 1. Decomposition of the $K^+ - W$ ion-atom exchange repulsions in electronic kinetic energy terms and in Coulomb terms [38]

r (Å)	Kinetic energy (eV)	Coulomb energy (eV)
1.06	635	-436
1.59	251	-211
2.24	66.7	-62.6
3.18	13.1	-14.4

The $\Delta\varrho^0$ plot of Fig. 4 is in fact a clear illustration of the deviation from $\varrho_A + \varrho_B$ induced by the Pauli exclusion principle which requires zero probability of finding two electrons of the same spin at the same position.

In solids, this effect is often referred to as Born repulsion. In the work by Bagus et al. [28], ΔE^0 is called the frozen orbital energy, in agreement with Eq. (1) for Ψ^0 . However, one should not infer from this name that the charge densities are frozen, and in particular the terminology "charge superposition repulsion" [29] should be avoided, leading to misunderstandings as to the real cause of the effect.

The exchange repulsion plays a very significant role in chemical interactions (refer to [40] for an extensive discussion). It is to be noted that the ubiquitous steric hindrance effects are not due to Coulombic repulsions but are due to the Pauli repulsion. ΔE^0 , comprising both the attractive Coulombic interactions and the exchange repulsion, is appropriately called steric repulsion. Apart from the action of exchange repulsion at the outer edges of the molecular electron distributions to provide steric hindrance and the repulsive part of the potential in, e.g., molecular interactions (Van der Waals complexes), it is also very important in determining bond distances. The exchange repulsion of occupied valence orbitals on one fragment with subvalence (semi-core) orbitals on the other fragment is responsible for the repulsive part of the potential energy curve determining the distance.

When we consider the simple two-orbital model used before, it is clear that the kinetic energy increases due to the orthogonalization of ϕ_B to φ_A to yield ϕ'_B , by an amount of approximately $S^2 \langle \varphi_A | T | \varphi_A \rangle$. This rise in kinetic energy is important if φ_A has a high kinetic energy, which is increasingly so for the deep lying doubly occupied core orbitals, and if S is not too small, i.e. if the core orbital is not too contracted. This leads e.g. in the case of CO interacting with a transition metal atom of the third row to the largest contribution to the kinetic repulsion coming from the orthogonalization of the rather bulky C lone pair orbital (5σ) on the 3s, 3p subvalence orbitals.

It has been pointed out in Ref. [26] that this is a short-range, local effect. Therefore, clusters of metal atoms modelling chemisorption by containing at least all the nearest neighbors of an adsorbate yield in general quite reasonable adsorbate surface distances, even if the total chemisorption energy may be quite different.

Apart from the exchange repulsion between valence and semi-core levels, there is of course also exchange repulsion between occupied valence levels. For instance, if the 4s shell is occupied, as it is in most free transition-metal atoms of the third row,

there is a very large exchange repulsion with the lone-pair orbitals on ligands [24, 25]. For this reason the effective configuration of the transition-metal atom changes from $3d^n 4s^2$ in the free atom to $3d^{n+2} 4s^0$ in complexes.

In the same way, there is exchange repulsion of lone pair orbitals on adsorbates and the occupied conduction electron levels in a metal. This effect is more important if the conduction electron density is higher. It has been pointed out by Post and Baerends [41] that the much higher conduction electron density of Al (3 valence electrons) compared to Li (1 valence electron) leads to much stronger 5σ /metal- s_p exchange repulsion with CO for Al than Li. Bagus et al. [30] have stressed this " σ -repulsion" for CO interacting with metals.

We next turn to the orbital interactions that change the repulsive wave function Ψ^0 in the fully converged Hartree-Fock one-determinantal ground state wave function Ψ_{conv} resulting in covalent bonding. It is common to distinguish between polarization-type interactions, which result from mixing virtual orbitals on A into occupied orbitals on A, and similar for B, and charge-transfer type of interaction consisting of admixture of A virtuals into occupied B levels and vice versa (cf. Fig. 5a). Although the final wave functions is well-defined, as is Ψ^0 , the steps in between are not unique. It is immediately evident that if a complete basis is used to describe system A, the sum of occupied and virtual spaces on A necessarily includes the full B space, and, e.g., polarization of A and charge transfer from A to B cannot be distinguished. Apart from this fundamental ambiguity caused by the overlap between the A and B orbital spaces, there is also a dependency of the results of the charge transfer/polarization analysis depending on the way the overlap is treated in practice.

In the original Morokuma scheme [15], the matrix of Hamiltonian interaction elements (Fock matrix) and the overlap matrix in the secular equation:

$$(F - ES)C = 0 \quad (4)$$

are treated simultaneously. For instance, the steric repulsion is evaluated by retaining only matrix elements of both F and S amongst occupied orbitals, and setting all matrix elements connecting an occupied orbital to a virtual empty orbital to zero. This is of course equivalent to the orthogonalization of occupied orbitals discussed before, as diagonalization of F is nothing but a unitary transformation amongst the orthogonalized orbitals. In this way canonical orbitals are obtained for Ψ^0 characterized by their orbital energies.

In Fig. 5b this is shown schematically for the three-orbital system: stabilized bonding and destabilized antibonding combinations are formed. In a one-electron picture the repulsive character of ΔE^0 is reflected in a stronger destabilization of ψ'_B and χ'_B than stabilization of ϕ'_A (see below).

In order to include, e.g., A to B charge transfer, Morokuma et al. allow, apart from the matrix elements of the Ψ^0 step, also the matrix elements of both F and S among the virtual B orbitals and the matrix elements connecting the virtual B and occupied A orbitals to be non-zero. In a similar way, other contributions such as polarization of B, or charge transfer of B to A, etc. are determined in separate calculations.

In general, the sum of the individual energy contributions differs from the result obtained when allowing all the interactions to take place simultaneously, which is in

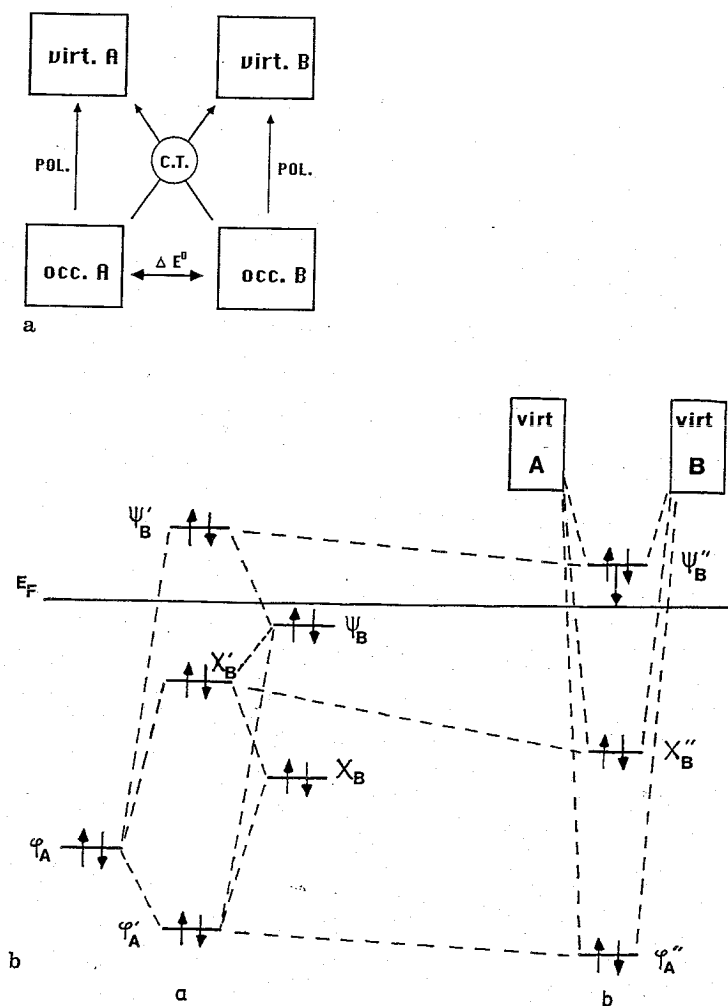


Fig. 5a. Schematic interaction scheme of fragments A and B, indicating polarization and charge transfer interactions. **b** Interaction diagram for the orbital interactions of two interacting units A and B (in the presence of a metal surface). A contains one orbital φ_B , B contains two orbitals χ_B and ψ_B . a. One electron energies of orbitals forming Ψ^0 . b. One electron energies of orbitals forming Ψ_{conv} .

accordance which the intuitive concept of synergism of, e.g., donation and back-donation (see for a detailed analysis of synergic effects in metal-ligand bonding Ref [25]).

Bagus et al. have chosen to treat the overlap in a different way. They chose a specific order in which they (Schmidt) orthogonalize the orbitals on all the previous ones, e.g., (occ A) + (occ. B) + (virt. B) + (virt. A). In the Fock matrix in this basis, in which the overlap S matrix is diagonal, blocks are successively allowed to be non-zero. After the Ψ^0 step based on (occ. A) + (occ. B) only, the set (virt. B) is allowed to mix

with the set (occ. B). Note that both (occ. B) and (virt. B) now refer to sets Schmidt-orthogonalized on (occ. A). This mixing leads to polarization of B in the field of unmodified A (the set (occ. A), being first in the Schmidt-orthogonalization process, is unchanged). Note that the resulting polarization of B is not only due to an electrostatic field, but is also the result of orthogonalization of the full set B on (occ. A). This will be discussed in more detail below. So the polarization concerned is not just classical polarization in an electrostatic field. If the interaction of (occ. B) with (virt. A) is added, also electron donation from B to A is allowed to take place. This process may be continued, for instance, polarization of A in the field of the relaxed B fragment that has been obtained after the previous steps, with relaxed occupied orbitals (occ. B'), may be obtained by allowing (virt. A), now Schmidt-orthogonalized to (occ. B'), to interact with (occ. A). The energy will be lowered in each step, and finally the fully converged SCF energy will be reached. The procedure is clearly asymmetrical, the steps are consecutive. The dependance of the results on the chosen order in what are called CSOV steps (Constrained Space Orbital Variation) has been discussed by Bauschlicher [42].

Yet another way to decompose the electronic interaction energy, i.e., charge transfer plus polarization energies, is based on symmetry. Only A- and B-orbitals belonging to the same irreducible representation will interact. This is the basis for the widely used distinction between, e.g., σ -donation and π -backdonation. It is indeed possible to write the total electronic interaction energy as the sum of contributions from the irreducible representations. We may write:

$$\begin{aligned}\Delta E_{\text{int}} &= E(\Psi_{\text{conv.}}) - E(\Psi^0) \\ &= \frac{1}{2} \sum_{\mu, \nu} P_{\mu\nu} (H_{\mu\nu}^{\text{core}} + F_{\mu\nu}) - \frac{1}{2} \sum_{\mu, \nu} P_{\mu\nu}^0 (H_{\mu\nu}^{\text{core}} + F_{\mu\nu}^0)\end{aligned}$$

where H^{core} is the matrix of the purely one-electron operators (kinetic energy and nuclear attraction energy) in Hartree-Fock or the effective core Hamiltonian in semi-empirical schemes, and F is the Fock matrix. As all of the matrices in this expression are symmetry blocked, this means:

$$\Delta E_{\text{int}} = \sum_{\Gamma} E_{\Gamma}$$

It has been shown by Ziegler and Rauk [43] that ΔE^{int} may, to a good approximation, be expressed in terms of $\Delta P_{\mu\nu} = P_{\mu\nu} - P_{\mu\nu}^0$ and an effective Fock matrix F^{eff} :

$$\Delta E_{\text{int}} = \sum_{\Gamma} \sum_{\mu, \nu} \Delta P_{\mu\nu}(\Gamma) F_{\mu\nu}^{\text{eff}}(\Gamma)$$

where $F_{\mu\nu}^{\text{eff}}(\Gamma)$ is an average over the initial F^0 , the final F , and an intermediate "transition state" Fock matrix F^{TS} .

The symmetry decomposition is unambiguous. The arbitrariness involved in the distinction between charge transfer and polarization is not present in the symmetry separation.

It should also be noted that the results of a symmetry analysis cannot be compared directly to the results of the previous schemes. A contribution of a given symmetry will in general contain *both* charge transfer and polarization. The symmetry analysis has been introduced by Ziegler [43] and has been applied extensively to transition-metal complexes [22, 23, 25] and to cluster studies of chemisorption [26, 41].

The effect of charge transfer and polarization, i.e., the mixing of virtual orbitals into the levels that have been formed in the steric repulsion step (Ψ^0) is schematically shown in Fig. 5b (to the right). All of the levels ϕ'_A , χ'_B , and ψ'_B will be stabilized, if symmetry permits, but in particular this will be the case for the high-lying ψ'_B .

We would like to stress that one of the most important results of the polarization is the reduction of Pauli repulsion. An example is the interaction of system A with a low-lying (semi-core) orbital ϕ_A with system B having a valence s-orbital ψ_B (cf. Fig. 5b) and an additional virtual p-level ψ_{vB} . ψ_{vB} represents a level of the block virt-B in Fig. 5b. If the energy separation between ψ_B and ϕ_A is large, in particular if the interaction matrix element is negligible compared to the energy separation, the canonical orbital resulting in the Pauli repulsion step from the diagonalization of the Fock matrix in the space of occupied orbitals only (cf. Fig. 5b(a)) will be practically identical to the simple Schmidt-orthogonalized orbital (see Fig. 6):

$$\psi'_B = (\psi_B - S\phi_A) / \sqrt{(1 - S^2)}$$

As pointed out before, the energy of this orbital will still be raised due to a possibly large kinetic energy of ϕ_A .

In the subsequent polarization step of allowing admixture of ψ_{vB} into the occupied B-space, we obtain the following coupling matrix element between ψ_{vB} and ψ'_B :

$$\langle \psi_{vB} | H_{\text{eff}} | \psi'_B \rangle = \frac{1}{\sqrt{(1 - S^2)}} [\langle \psi_{vB} | H_{\text{eff}} | \psi_B \rangle - S \langle \psi_{vB} | H_{\text{eff}} | \phi_A \rangle]$$

Here, H_{eff} represents the effective Hamiltonian operator of the one-electron model used.

If the model used is the Hartree-Fock approximation, H_{eff} contains explicitly the field of all the electrons and nuclei in the system. Therefore, the first matrix element in the square brackets represents the coupling of the virtual B orbital to the occupied one because the effective field has changed from the one for isolated B (in which case this matrix element is zero) due to the presence of system A.

System A will exert a direct electrostatic field, particularly if it is not neutral. We are here dealing with the common electric polarization of system B in an external field. [The charge rearrangement occurring in the Pauli repulsion (cf. Fig. 4) of course modifies the field from what it would be if the charges of A and B were simply superimposed].

It is clear, however, that there is another contribution to the polarization which does not have such a simple electrostatic interpretation. This is due to the second matrix element in the square brackets. This part of the polarization has its origin in the orthogonalization or Pauli repulsion, as is evident from the proportionality with the overlap S . It couples the virtual B state to the occupied one through the contamination of the latter with ϕ_A . It is to be noted that in simple one-electron methods which do not incorporate electrostatic fields due to neighboring moieties (Hückel, extended Hückel), the electric polarization is absent. However, as soon as overlaps are taken into account (extended Hückel), the polarization that relieves the Pauli repulsion will be in effect. Figure 6 illustrates this type of polarization. It can easily be deduced from the sign of the matrix element given above that the admixing of the p-type ψ_{vB} into ψ'_B is such that the original occupied s-type ψ_B hybridizes away from the overlap region so as to alleviate the antibonding with ϕ_A .

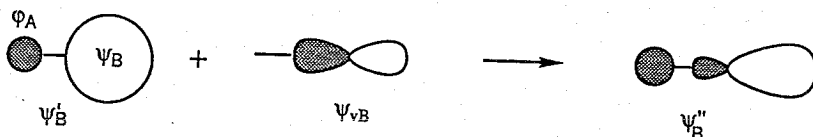


Fig. 6. Polarization due to admixture of virtual p orbital ψ_{vB} into the orthogonalized (onto ϕ_A) s orbital ψ'_B

The charge rearrangement in this polarization is such that the electron density becomes more smooth. The strong removal of charge from the overlap region and piling up on A and B which is characteristic of the Pauli repulsion is counteracted by a flow of charge back into the overlap region so that the overlap population becomes less negative, a reduction of the net populations of ϕ_A and ψ_B and an increase of charge at the back of B due to population of ψ_{vB} .

As methods like the extended Hückel are very suitable to obtain insight into the symmetry aspects of orbital interaction, it is important to realize in which way and to what extent the physics of the interaction that has been discussed in this section is embodied in such a method. In Sect. 2.3, we will therefore discuss in some detail, for several model systems, extended Hückel calculations from the point of view developed here.

Another important aspect of interaction of molecules with infinite systems is that in the presence of a Fermi level, as soon as an antibonding level ψ'_B is lifted above the Fermi energy, the Pauli repulsion will immediately be relieved by deexcitation of the electrons to the Fermi level. In Fig. 5b(b) such a deexcitation is indicated. This is an important difference with finite systems where low-lying empty levels to receive the electrons will not always be present. In that case, considerable repulsion (antibonding interaction) will have to develop before level ψ'_B becomes sufficiently destabilized to lose its electrons to another B orbital. As will be discussed in Sect. 3.1, this situation occurs frequently in interactions of molecules with transition-metal atoms (i.e., fragments), where the ns orbital loses its electrons to the $(n-1)d$, which corresponds to an excitation in the free atom (promotion energy). At a surface or

on clusters, frontier orbital interactions that may lead to bond breaking may meet with a lower activation barrier simply because the opposing repulsive forces develop less strength. We will return to this point in Sect. 3.3.

For finite systems, polarization, i.e., the admixture of virtual orbitals, decreases the Pauli-repulsion effects experienced by the occupied orbitals.

As discussed, the admixture of virtual and occupied orbitals on the same fragment arises mainly from non-orthogonality of the orbitals on different fragments at short distance. Only for charged fragments and if bonding distances become such that overlap of fragment orbitals becomes very small, polarization of the fragments will be found to be due to each others electrostatic field.

2.2 The Extended Hückel Method

In the extended Hückel method [44], molecular orbitals are expanded in a minimum basis set.

The diagonal and non-diagonal matrix elements of the Hamiltonian become:

$$\langle \varphi_i | H | \varphi_j \rangle = \langle \varphi_i | \hat{T}(\vec{r}) - \sum_A \frac{Z_A e^2}{|\vec{R}_A - \vec{r}|} + e^2 \int d\vec{r}' \frac{\rho(\vec{r}')}{|\vec{r} - \vec{r}'|} - E(\text{exch}, \vec{r}) | \varphi_j \rangle \quad (5)$$

\hat{T} is the kinetic energy operator and $E(\text{exch}, \vec{r})$ the contribution to the exchange energy.

The exchange energy contribution to Eq. (5) is due to the modification of the electron-electron interaction energy because of the requirement that the multielectron wave function must be antisymmetric.

In the extended Hückel method, the repulsion which the electron experiences from electrons on neighboring atoms is supposed to be cancelled by the attraction with the nuclei. In addition, the electron-electron interactions on one atom are averaged or simulated by an electron density-dependent term (iterative extended Hückel).

The first assumption implies that the atoms are considered to be neutral. The total energy is simply the sum of the occupied molecular orbitals.

The diagonal elements of the Hamiltonian matrix become:

$$\langle \varphi_{i,A} | H | \varphi_{i,A} \rangle = \langle \varphi_{i,A} | \hat{T}(\vec{r}) - \frac{Z_A^{\text{eff}}}{|\vec{R}_A - \vec{r}|} | \varphi_{i,A} \rangle \quad (6a)$$

The non-diagonal matrix elements are approximated by:

$$\begin{aligned} \langle \varphi_{i,A} | H | \varphi_{j,B} \rangle = & \frac{1}{2} \langle \varphi_{i,A} | \varphi_{j,B} \rangle \{ \langle \varphi_{i,A} | H | \varphi_{i,A} \rangle + \langle \varphi_{j,B} | H | \varphi_{j,B} \rangle \} \\ & + \langle \varphi_{i,A} | \hat{T} | \varphi_{j,B} \rangle - \frac{1}{2} \langle \varphi_{i,A} | \varphi_{j,B} \rangle \{ \langle \varphi_{i,A} | \hat{T} | \varphi_{i,A} \rangle + \\ & + \langle \varphi_{j,B} | \hat{T} | \varphi_{j,B} \rangle \} \end{aligned} \quad (6b)$$

Equation (6b) is derived from Eq. (6a) by expanding $\varphi_{i,A}$ and $\varphi_{j,B}$ into a complete set of basis functions on the other atom and only retaining the terms containing

diagonal Hamiltonian matrix elements. Since this approximation induces a significant error in the kinetic energy term, the kinetic energy term has to be corrected for.

It will be shown later that the second part of Eq. (6b) governs the attractive part of the covalent bond strength.

Equations (6a) and (6b) are often replaced by empirical values.

Anderson [45] corrects for the non-cancellation of nuclear attraction and electron repulsion for neutral atoms by adding in the total energy expression a semi-empirical repulsive expression to the attractive component of the total energy computed as the sum of the energies of the occupied molecular orbitals.

One can incorporate effects due to non-neutrality of charge, by maintaining Eqs. (6a) and (6b) for the matrix elements of the Hamiltonian, but adding to the total energy expression a Madelung potential energy term.

An analysis of modifications of the extended Hückel method which also applies to the recombination of radicals and where changes in electron-electron interaction are important, can be found in Ref [46].

2.3 The Effect of Overlap on the Bond Energy According to the Extended Hückel Method

The polarization effects compensating partly for exchange repulsion in the frozen orbital approximation discussed earlier are also found in the extended Hückel method.

In the extended Hückel method, molecular orbitals are derived by solving the matrix equation:

$$[H - ES]c = 0 \quad (7a)$$

The difference between the solutions of Eq. (7a) and Eq. (7b):

$$[H - EI]c = 0 \quad (7b)$$

with I the unit matrix, will be described with the aim of studying the role of non-orthogonality of the basis functions φ_i . Equation (7b) is used in the Hückel method.

Let us first recall the simple case of a homonuclear diatomic molecule B-B, each atom B with one atomic orbital of energy α and with a coupling matrix element β and overlap S . The molecular orbital energies, corresponding to bonding and anti-bonding combinations $\psi_{\pm} = (\varphi_1 \pm \varphi_2)/\sqrt{2 \pm 2S}$, are:

$$\varepsilon_{\pm} = \frac{\alpha - S\beta}{1 - S^2} \pm \frac{\beta - \alpha S}{1 - S^2}$$

Comparing this to the values for $S = 0$, $\varepsilon_{\pm} = \alpha \pm \beta$, it is noted that S has two effects: the average energy of the two levels is raised, and the spacing between the levels is reduced.

The first effect causes, if four electrons are present so that both bonding and anti-bonding levels are filled, a repulsion $= -4S(\beta - \alpha S)/(1 - S^2)$. This is the steric repulsion of all-electron methods. It would clearly be absent here if S is neglected.

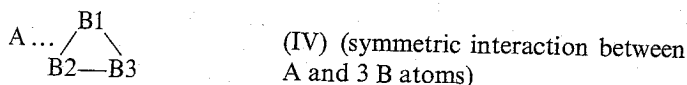
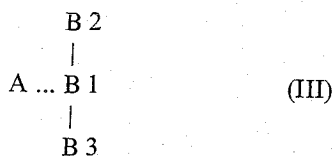
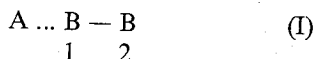
If we consider a two-electron bond, i.e., filling of the bonding orbital only, the bond energy appears to be reduced by $-2S(\beta - \alpha S)/(1 - S^2)$ because of the raising of the average level energy and, in addition, it becomes less because β is reduced by $-\alpha S$.

The bondenergy becomes $\Delta E = \{-2S(\beta - \alpha S) + 2(\beta - \alpha S)\}/(1 - S^2) = \frac{2(\beta - \alpha S)}{1 + S}$.

These effects of the overlap are general.

In the following, this will be shown for a few simple model systems that can be readily analyzed.

The interaction is described according to the extended Hückel method of the following model systems and configurations:



The fragments B-B, B-B-B, and $\begin{array}{c} \text{B} \\ \diagdown \quad \diagup \\ \text{B} - \text{B} \end{array}$ are described within the Hückel approximation implying that atomic orbitals $\varphi_{\text{B}}(i)$ are orthogonal. A minimum basis set is assumed, with one atomic orbital per atom of s symmetry, denoted by φ_{A} and $\varphi_{\text{B}}(i)$.

The diagonal matrix elements of the Hamiltonian are supposed to be equal:

$$\langle \varphi_{\text{A}} | \text{H} | \varphi_{\text{A}} \rangle = \langle \varphi_{\text{B}}(i) | \text{H} | \varphi_{\text{B}}(i) \rangle = \alpha$$

The following parametrizations for the different systems apply:

$$\text{I.} \quad \langle \varphi_{\text{A}} | \text{H} | \varphi_{\text{B}}(1) \rangle = \beta' \quad ; \quad \langle \varphi_{\text{A}} | \text{H} | \varphi_{\text{B}}(2) \rangle = 0$$

$$\langle \varphi_{\text{B}}(1) | \text{H} | \varphi_{\text{B}}(2) \rangle = \beta$$

$$\langle \varphi_{\text{A}} | \varphi_{\text{B}}(1) \rangle = S$$

$$\langle \varphi_{\text{A}} | \varphi_{\text{B}}(2) \rangle = 0$$

$$\text{II.} \quad \langle \varphi_{\text{A}} | \text{H} | \varphi_{\text{B}}(1) \rangle = \langle \varphi_{\text{A}} | \text{H} | \varphi_{\text{B}}(2) \rangle = \beta'$$

$$\langle \varphi_{\text{B}}(1) | \text{H} | \varphi_{\text{B}}(2) \rangle = \beta$$

$$\langle \varphi_{\text{A}} | \varphi_{\text{B}}(1) \rangle = \langle \varphi_{\text{A}} | \varphi_{\text{B}}(2) \rangle = S$$

- III. $\langle \varphi_A | H | \varphi_B(1) \rangle = \beta'$
 $\langle \varphi_A | \varphi_B(1) \rangle = S$
 $\langle \varphi_A | \varphi_B(2) \rangle = \langle \varphi_A | \varphi_B(3) \rangle = 0$
 $\langle \varphi_B(1) | H | \varphi_B(2) \rangle = \langle \varphi_B(1) | H | \varphi_B(3) \rangle = \beta$
- IV. $\langle \varphi_A | H | \varphi_B(1) \rangle = \langle \varphi_A | H | \varphi_B(2) \rangle = \langle \varphi_A | H | \varphi_B(3) \rangle = \beta'$
 $\langle \varphi_A | \varphi_B(1) \rangle = \langle \varphi_A | \varphi_B(2) \rangle = \langle \varphi_A | \varphi_B(3) \rangle = S$
 $\langle \varphi_B(1) | H | \varphi_B(2) \rangle = \langle \varphi_B(1) | H | \varphi_B(3) \rangle = \langle \varphi_B(2) | H | \varphi_B(3) \rangle = \beta$

Case I assumes the interaction of a doubly occupied φ_A at energy α with a doubly occupied bonding B-B orbital $\varphi^+ = (\varphi_{B1} + \varphi_{B2})/\sqrt{2}$ at energy $\alpha + \beta$ (see Fig. 7).

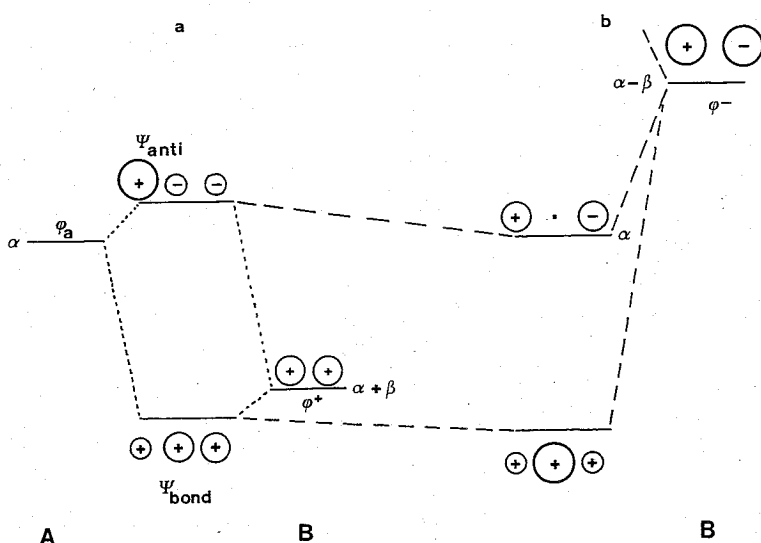


Fig. 7 a, b. Interaction of fragment A with orbital φ_a with fragment B having one double occupied orbital φ^+ of s symmetry and an unoccupied orbital φ^- of p symmetry. a Interaction between φ_a and occupied orbital φ^+ only. b Effect of additional interaction with virtual orbital φ^-

As expected, there is repulsion which is found to be, to lowest order in S , $-2\left(\beta' - \frac{1}{2}(2\alpha + \beta)S\right)S$. Evidently, since both the bonding combination:

$$\psi_{\text{bond}} = c_A \varphi_A + c_+ \varphi^+$$

and the antibonding combination:

$$\psi_{\text{anti}} = \frac{(C_+ + C_A S/\sqrt{2})}{\sqrt{(1 - S^2/2)}} \varphi_A - \frac{(C_A + C_+ S/\sqrt{2})}{\sqrt{(1 - S^2/2)}} \varphi^+$$

are occupied, the gross populations of φ_A and φ^+ are 2.0.

The charge rearrangements that accompany the repulsion are therefore not visible in the gross populations, but they do show up in the net populations. To second order in S , the net populations of φ_A and φ^+ are $2 + S^2$ and there is a total negative overlap population of $-2S^2$.

It is interesting to consider also the charge distribution within B-B. As the coefficients of B_1 and B_2 are equal to each other in both ψ_{bond} and ψ_{anti} (as depicted in Fig. 7) the total net populations of φ_{B1} and φ_{B2} are equal, viz. $1 + S^2/2$. For φ_{B2} this is also the gross population, but for φ_{B1} there is an overlap population contribution with φ_A which is positive and of first order in S in the bonding orbital ψ_{bond} but negative in ψ_{anti} . The first-order contribution in ψ_{anti} cancels the one in ψ_{bond} and the total overlap population contribution for φ_{B1} is $-S^2$, yielding a gross population of $1 - S^2/2$. The gross and overlap populations clearly fit in with the charge distributions expected from the discussion in Sect. 2.1 for the Pauli-repulsion step, but only if the overlap S is taken into account.

Subsequently, the orbital φ^- on B-B is allowed to mix in. Both charge-transfer- and polarization-type of mixing (which are not distinguished here; see the remark at the end of Sect. 2.1) into ψ_{bond} and ψ_{anti} will cause the ratio of the coefficients of φ_{B1} and φ_{B2} to increase in ψ_{bond} and to decrease in ψ_{anti} . The results for the present case (I) and the other cases may be obtained from full solutions of the secular equations.

For case I the solution for the molecular orbital energies is:

$$E_{1,3} = \frac{\alpha - S\beta'}{1 - S^2} \pm \frac{1}{1 - S^2} [(1 - S^2)\beta^2 + (\beta' - \alpha S)^2]^{1/2} \quad (8a)$$

$$= \frac{\alpha - S\beta'}{1 - S^2} \pm \Delta \quad (8b)$$

$$E_2 = \alpha$$

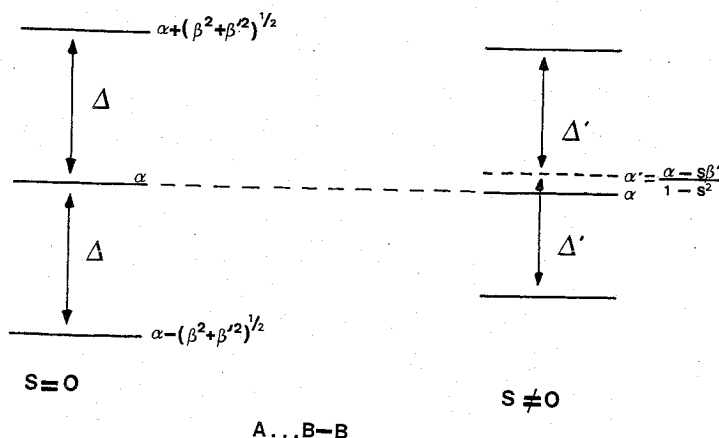


Fig. 8. A ... B-B Molecular Orbital Scheme

The solutions for case III are completely analogous, with β replaced by $\beta/\sqrt{2}$. Since β' also depends on S , these parameters cannot be chosen independently. Physical solutions to Eq. (8) only exist if:

$$\left| \frac{\alpha - S\beta'}{1 - S^2} \right| < |\alpha| \quad \text{and} \quad \frac{1}{1 - S^2} [(1 - S^2)\beta^2 + (\beta' - \alpha S)^2]^{1/2} < (\beta^2 + \beta'^2)^{1/2}$$

In Fig. 8 the solutions for the molecular orbital energies are compared for $S = 0$ and $S \neq 0$ in Eq. (8).

Figure 8 also reveals that (as always) the condition $S \neq 0$ raises the average position of the molecular levels and decreases the dispersion Δ of the molecular orbital levels. As observed in Eq. (8), the dispersion decrease is of the order αS . So, two effects of S decrease the interaction energy.

- a) $|\alpha'| < |\alpha|$, cf. increase of kinetic energy by Pauli repulsion.
- b) $|\Delta'| < |\Delta|$, decrease of covalent bonding.

In case I the ratio of the net populations (coefficients squared) on the two B atoms in molecular orbital i now differs from 1. It is given by:

$$\frac{q_B^i(2)}{q_B^i(1)} = \frac{\beta^2}{|\alpha - E_i|^2}$$

It follows that the coefficient of atom 1 in the orbital at energy α , which is ψ_{anti} stabilized by interaction with φ^- (see Fig. 7b), is zero. This is the well-known node in the nonbonding orbital at the central atom of the symmetrical allylic system, which is here shown to occur also if $\beta' \neq \beta$.

Whereas both the net population of $\varphi_{B1}(1)$ and the negative overlap population with φ_A in this orbital thus disappear, the reverse effects take place in the lowest orbital derived from ψ_{bond} .

The precise charge redistribution upon allowing φ^- to interact is subtle. If fragment B contains two electrons, there is polarization of B-B away from A, but the polarized system has stronger bonding (particularly less antibonding) to A. Apart from this, it is interesting to note that since $|\alpha - E_1'| < |\alpha - E_1|$, comparing the cases $S \neq 0$ and $S = 0$ for the full solutions of the three-orbital system, there is a shift in the net population in the lowest orbital towards atom 2 if S differs from zero. At the same time, of course, an overlap population contribution to the gross population of $\varphi_B(1)$ appears when $S \neq 0$.

The molecular orbital energies for cases II and IV are also readily found:

$$E^\pm = \frac{\alpha + \frac{n}{2}\beta - Z\beta'S}{(1 - ZS^2)} \pm \frac{1}{2(1 - ZS^2)} \times [n^2\beta^2 + 4\alpha nZ\beta^2S - 4nZ\beta\beta'S + 4Z(\beta' - \alpha S)^2]^{1/2} \quad (9)$$

$$n = Z - 1.$$

In case II, $n = 1$, $Z = 2$; In case IV, $n = 2$, $Z = 3$.

In case II the third level has energy $\alpha - \beta$.

In case IV, in addition to levels E^\pm , two MOs with energy values $\alpha - \beta$ are found.

The general result is similar to that found for cases I and III discussed earlier.

The Pauli repulsion term is proportional to Z , the number of atoms on B that are the next neighbor of A.

If molecule B contributes two electrons, the Pauli repulsion energy becomes:

$$E_{\text{rep}}^p \approx -ZS(\beta' - \alpha S) \quad (10)$$

Concerning the terms giving dispersion it is noteworthy that again, β' is replaced by $\beta' - \alpha S$ in Eqs. (8a) and (9) if $S \neq 0$.

As a consequence if $S \neq 0$, the first term of Eq. (6b) for the nondiagonal matrix element of the Hamiltonian cancels in the eigenvalue equation and bonding is governed by the second term in Eq. (6b).

This can be easily proven for the general case of an array of equal atoms and s type nonorthogonal atomic orbitals with only nearest neighbor interactions. The expressions for the molecular orbitals are:

$$\psi_k = \frac{1}{\left[\sum_i c_i^{k2} + 2 \sum_{i < j} c_i^k c_j^k S_{ij} \right]^{1/2}} \sum_j c_j^k \varphi_j \quad (11a)$$

$$\psi_k = \sum_j u_j^k \varphi_j \quad (11b)$$

and for the molecular orbital energy:

$$E_k = \sum_i u_i^{k2} \alpha_i + 2 \sum_{i < j} u_i^k u_j^k \beta_{ij} \quad (12a)$$

$$= \sum_i \alpha_i \left(u_i^{k2} + \sum_{j \neq i} u_i^k u_j^k S_{ij} \right) + 2 \sum_{i < j} u_i^k u_j^k \left(\beta_{ij} - \frac{1}{2} (\alpha_i + \alpha_j) S_{ij} \right) \quad (12b)$$

$$= \alpha + 2 \sum_{i < j} u_i^k u_j^k (\beta_{ij} - \alpha S_{ij}) \quad (12c)$$

Equations (12b) and (12c) illustrate the reduction of β_{ij} with $\frac{1}{2} (\alpha_j + \alpha_i) S_{ij}$.

Equation (12c) also shows that the weight of α_i is given by a Mulliken gross population of atomic orbital φ_i in molecular orbital k . For equal α , it becomes 1 by normalization.

Equation (12b) shows the crucial role of the bond-order term to chemical bonding. The bond order of atomic orbitals i and j is given by:

$$P_{ij} = \sum_k^{\text{occ}} u_i^k u_j^k$$

For a more general discussion see Ref [46].

Equation (9b) can be used to derive useful expressions for the bond energy as a function of $\bar{\beta}'/\beta$, the ratio of the effective interaction between atoms A and B and that between the B atoms ($\bar{\beta}' = \beta' - \alpha S$).

If $\bar{\beta}'/\beta \ll 1$, one finds for A symmetrically coordinated to a ring of interacting B atoms.

$$E_{\text{attr}} = \frac{-Z\bar{\beta}^2}{2|\beta|} \quad (Z > 2) \quad (13)$$

If $\bar{\beta}'/\beta \gg 1$, this contribution becomes:

$$E_{\text{attr}} \approx Z^{1/2}\bar{\beta}' \quad (14)$$

For weak bonding ($\bar{\beta}'/\beta < 1$), low coordination appears to be favored, since comparison with Eq. (10) shows the much stronger coordination-number dependence of the repulsive term compared to the attractive terms.

We will return to this interesting observation at a later point.

The considerations so far have not taken into account directional effects of atomic orbitals, with angular momentum $l \neq 0$, which also will be discussed later.

The extended Hückel picture of bonding has been shown to be very similar to that found from rigorous first-principle calculations.

Bonding according to first-principle calculations has been interpreted such that explicit inclusion of overlap ($S \neq 0$) leads to repulsive effects between doubly occupied orbitals. These repulsive effects are reduced if unoccupied orbitals are available to depopulate doubly occupied repulsive orbitals either by polarization of fragments or charge transfer (Fig. 5). The extended Hückel method incorporates both effects, but they appear indirectly. When overlap is taken into account, we have shown that bonding is decreased by an upward shift of the energies of the orthogonalized fragment orbitals with respect to the nonorthogonalized orbitals and by reduction of the dispersive overlap energy integrals. The latter leads to reduction of bonding between partially occupied orbitals, and to repulsion if interaction occurs between doubly occupied orbitals. Clearly, the more unoccupied virtual orbitals are available, the more the repulsive interactions is counteracted. Within the same fragment this interaction is due to nonorthogonality of the unoccupied virtual orbitals and interacting occupied fragment orbitals.

As long as the differences between the discrete levels are large compared to the overlap energy matrix elements, second-order perturbation theory can be used to

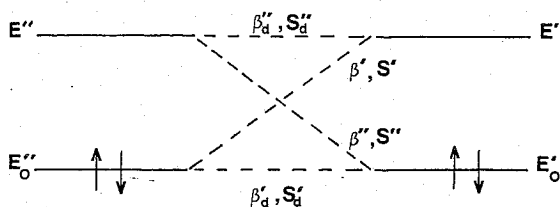


Fig. 9. Interaction energy and scheme according to second order perturbation theory

$$\Delta E = -4\beta'_d S'_d - 2 \frac{|\beta''_d - \frac{1}{2}(E' + E'_0) S''_d|^2}{E' - E'_0}$$

calculate the attractive contribution to the bond energy as in Eq. (13). The repulsive interaction term is calculated analogous as in Eq. (10). The formulae are illustrated in Fig. 9.

In the next section, techniques are discussed to compute the bond energy in case one of the fragments has a continuous energy spectrum, as for a metal surface.

2.4 Embedded Systems

A metal surface is part of a semi-infinite system. Apart from changes in electronic structure and electrostatics, a major difference between a finite and infinite system is, that there is no local conservation of the total number of electrons. The local number of electrons is determined by the requirement that for a system at equilibrium the Fermi-level energy, i.e., the energy of the Highest occupied molecular orbital is the same throughout the system.

The second qualitative difference between a finite and infinite system is that for a finite system, the electron energy spectrum is discrete, whereas for an infinite system, it is continuous, even though localized states may exist. Especially for the valence electron bands of metals with a low electron density, as a consequence, the electron energy spectrum slowly converges with increasing particle size to that of the infinite system.

In semi-infinite systems it is required that the Fermi level does not change and this allows the development of convenient closed expressions for changes in energy due to surface-formation or chemisorption. Such expressions have been derived by Koutecky [47], Grimley [48], Schrieffer [49], and others [50].

According to the extended Hückel method, the change in energy is given by:

$$\Delta E = 2 \left\{ \sum_i^{\text{occ}'} E_i' - \sum_i^{\text{occ}} E_i \right\} \quad (15)$$

E_i' are the orbital eigenvalues after chemisorption, and E_i the orbital eigenvalues before interaction.

Defining the energy density of states $\varrho(E)$ as:

$$\varrho(E) = \sum_i \delta(E - E_i) \quad (16)$$

and using the semi-infiniteness of the system:

$$E_{F'} - E_F \ll E_F$$

as well as conservation of total number of electrons:

$$\int_{-\infty}^{E_{F'}} dE \varrho'(E) = \int_{-\infty}^{E_F} dE \varrho(E)$$

one finds for the energy change [49]:

$$\Delta E = 2 \int_{-\infty}^{E_F} dE (E - E_F) \Delta \varrho(E) \quad (17a)$$

$$= -2 \int_{-\infty}^{E_F} dE \Delta n(E) \quad (17b)$$

with $\Delta \varrho(E)$ the change in electron energy density, and $\Delta n(E)$ the change in number of electrons of energy E . Equation (17b) presents the expected result, that changes in energy are related to rearrangements of electrons over energy levels. Using Green's function techniques, elegant practical expressions for $\varrho(E)$ have been developed. In Ref [51], an application of such theories to the problem of CO chemisorption to transition metals can be found.

Closed expression derived for Eq. (17) are useful, but not very suitable if one wishes to interpret changes in chemical bonding in terms of changes in electron density on molecular fragments. For this purpose it is more convenient to return to Eq. (12) for the total energy of a system according to the extended Hückel method:

$$\Delta E = 2 \left\{ \sum_i \alpha_i \Delta q_i + 2 \sum_{i < i'} \Delta P_{ii'} \left\{ \beta_{ii'} - \frac{1}{2} S_{ii'} (\alpha_i + \alpha_{i'}) \right\} \right\} \quad (18a)$$

$$= 2 \left\{ \sum_i \alpha_i \Delta q_i + 2 \sum_{i < i'} \Delta P_{ii'} \bar{\beta}_{ii'} \right\} \quad (18b)$$

with Δq_i the change in electron density on atomic orbital i :

$$\Delta q_i = \sum_k^{occ'} \left\{ u_i^{k2} + \sum_{i' \neq i} u_i^k u_{i'}^k S_{ii'} \right\} + \quad (19a)$$

$$- \sum_k^{occ} \left\{ u_i^{k2} + \sum_{i' \neq i} u_i^k u_{i'}^k S_{ii'} \right\}$$

$$= q_i' - q_i \quad (19b)$$

and $\Delta P_{ii'}$ the change in bond order between atomic orbitals i and i' :

$$\Delta P_{ii'} = \sum_k^{occ'} u_i^k u_{i'}^k - \sum_i^{occ} u_i^k u_{i'}^k \quad (20)$$

$$= P_{ii'}' - P_{ii'}$$

Similar methods as used to calculate Eq. (17) can be used to compute the quantities according to Eqs. (19) and (20).

As already mentioned, the important difference in the electron distribution of discrete and extended systems is the continuous nature of the electron energy density spectrum. The discrete sums have therefore to be replaced by integrals [51]:

$$q_i = \int_{-\infty}^{E_F} \varrho_{ii}(E) dE + \sum_{i' \neq i} P_{i'} S_{ii'} \quad (20a)$$

$$P_{ii'} = \int_{-\infty}^{E_F} dE \varrho_{ii'}(E) \quad (20b)$$

and $\varrho_{ii}(E)$ can be calculated from:

$$\varrho_{ii'}(E) = \frac{1}{\pi} \text{Im} \lim_{\epsilon \rightarrow 0} [\mathbf{O}(E + i\epsilon) - \mathbf{ES}]_{ii'}^{-1} \quad (22)$$

The problem posed by embedding a cluster into an extended system is solved once the matrix $\mathbf{O}(E)$ is known.

When chemisorption to a metal surface is studied, the matrix $\mathbf{O}(E)$ is given by:

$$\mathbf{O} = \left[\begin{array}{c|c} \mathbf{H}_{\text{ads}} & \mathbf{H}_{\text{ads, latt}} \\ \hline \mathbf{H}_{\text{latt, ads}} & \mathbf{O}_{\text{latt}}(E) \end{array} \right]$$

Equations (22) as well as (17) can be evaluated using the local nature of electron density changes. The electron density changes disappear if one is more than a few atomic distances removed from the adsorbate.

The block \mathbf{H}_{ads} contains the Hamiltonian matrix elements of the adsorbate and those atoms close to the adsorbate on which there are changes in electron density compared to the situation before adsorption.

$\mathbf{O}_{\text{lattice}}$ contains those atoms that are unperturbed by the adsorbate.

Green's function techniques [48, 50, 52] can be used to reduce the infinite $\mathbf{O}_{\text{lattice}}$ matrix to a finite one. For instance, a typical diagonal matrix element of \mathbf{O}_{latt} has the form [51]:

$$O_{\text{latt}ij}(E) = H_{ij} - \sum_{\gamma', \gamma''} (H_{i\gamma'} - ES_{i\gamma'}) \bar{G}_{\gamma'\gamma''}(E) (H_{\gamma''j} - ES_{\gamma''j}) \quad (23)$$

$\bar{G}_{\gamma'\gamma''}(E)$ is a Green's function matrix element of the undisturbed lattice, from which interactions with the atoms contained in \mathbf{H}_{ads} are excluded.

When chemisorption is modelled by interaction of a hydrogen type adsorbate with a tight-binding (Hückel) s-valence electron metal surface, each metal atom contributes one atomic orbital and the hydrogen atom interacts with one surface atomic orbital. Using the Bethe lattice [54, 55, 56] approximation to calculate the Green's function matrix elements $\bar{G}_{\gamma'\gamma''}(E)$, expressions for $\varrho_{ii'}(E)$ are readily found. and the hydrogen atom interacts with one surface atomic orbital. Using the Bethe lattice [54, 55, 56] approximation to calculate the Green's function matrix elements $\bar{G}_{\gamma'\gamma''}(E)$, expressions for $\varrho_{ii'}(E)$ are readily found.

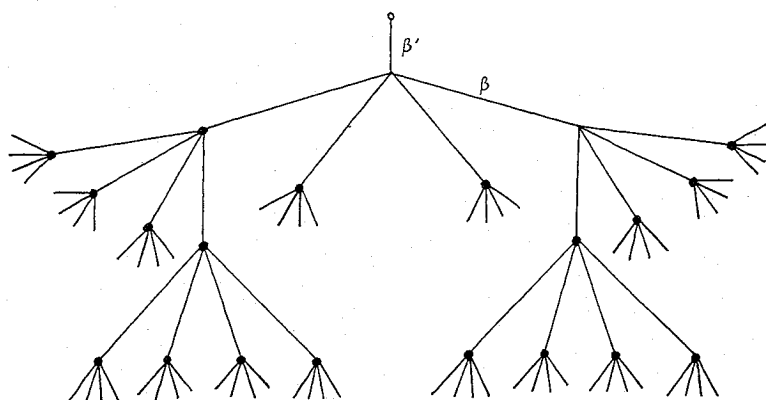


Fig. 10. Bethe lattice and adsorbed atom

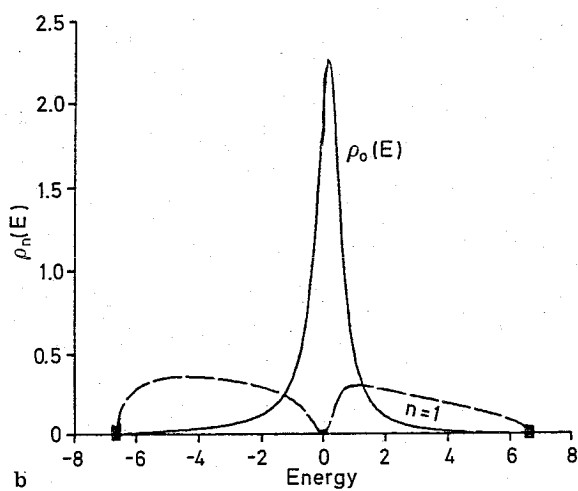
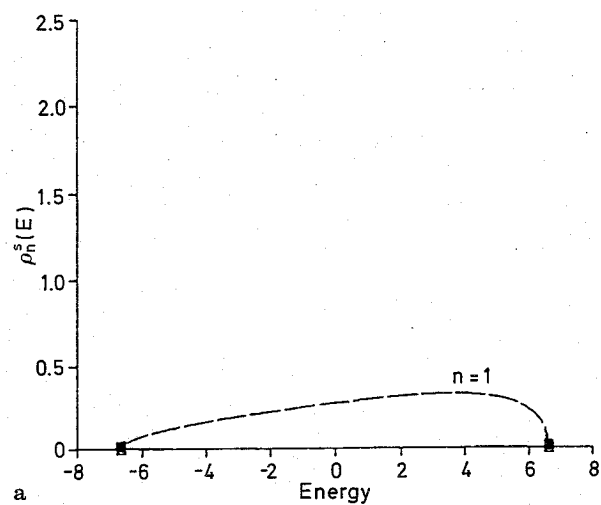


Fig. 11a. ρ_1 : Local electron energy density of states (LDOS) on metal atom to be bonded to hydrogen before adsorption; b ρ_0 : LDOS of adsorbed hydrogen atom, ρ_1 : LDOS on metal atom bonded to hydrogen after adsorption

$$\beta' = \beta = -1$$

$$\alpha_0 = \alpha_m$$

A Bethe lattice is sketched in Fig. 10. An adsorbed atom is represented by the open circle. Figure 11 b shows calculated electron energy density of states results for hydrogen adsorption. The calculations have been done assuming S in Eq. (22) to be the unit matrix. The Bethe lattice used simulates the (111) face of a f.c.c. crystal. All diagonal and non-diagonal matrix elements, respectively, are assumed to be equal. The number of lattice atom neighbors in the bulk is 12, at the surface it is 9.

As is shown in Fig. 11 b, the local electron energy density of states (LDOS) $\rho_0(E)$ at the hydrogen atom is found to be broadened into a Lorentzian curve.

The LDOS $\rho_0(E)$ has been extensively studied [49, 57]. If the coupling matrix element β' to the lattice atom is small compared to $2\beta\sqrt{Z}$, which is the Bethe lattice bandwidth ($Z + 1$ is number of bulk atom neighbors), then Eq. (22) reduces to a Lorentzian distribution:

$$\rho_0(E) = \frac{1}{\pi} \frac{\Gamma(E)}{(\alpha + \Lambda(E) - E)^2 + \Gamma^2(E)} \quad (26a)$$

For weak adsorption, $\Lambda(E)$ is small, and to lowest order, $\Gamma(E)$ is given by:

$$\Gamma = Z'\beta'^2 \bar{\rho}_1(E = \alpha) = \frac{Z'\beta'^2}{Z^{1/2}|\beta|} \quad (26b)$$

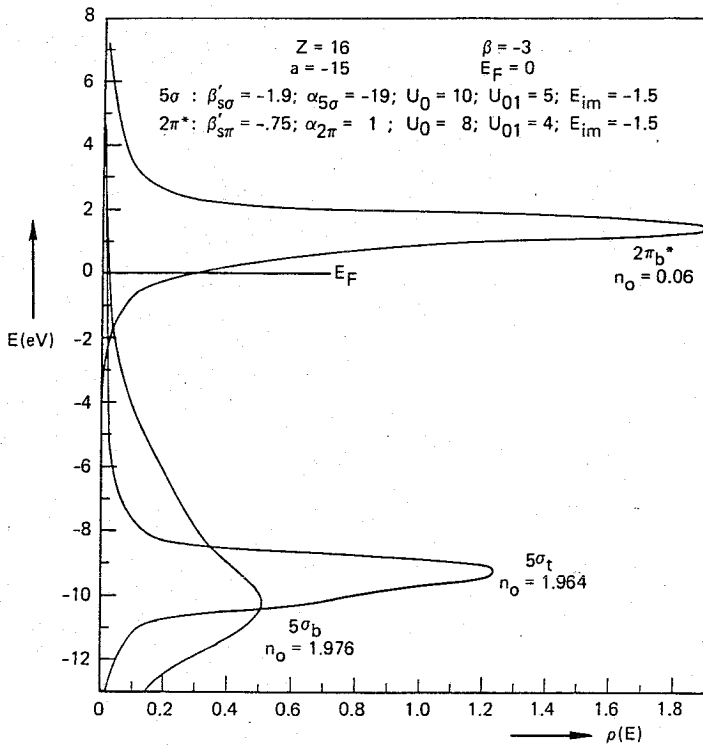


Fig. 12. LDOS $\rho_0(E)$ for the 5σ and $2\pi^*$ orbitals of CO adsorbed top(t) or three (b) coordinated the (111) surface of a s-band Bethe lattice f.c.c. metal [51]

Z' is the number of adsorbate atom neighbors, $\bar{\rho}_1(E = \alpha)$ the local density of states of the lattice atom orbital interacting with the adsorbate before adsorption.

The function $\bar{\rho}_1(E)$ will be discussed later.

Figure 12 illustrates computed adsorbate local density of states (LDOS) using a similar approximation (23) for σ and π symmetry orbitals of cote mono- or three-coordinated to the surface of an s-band model f.c.c. metal. As will be explained later

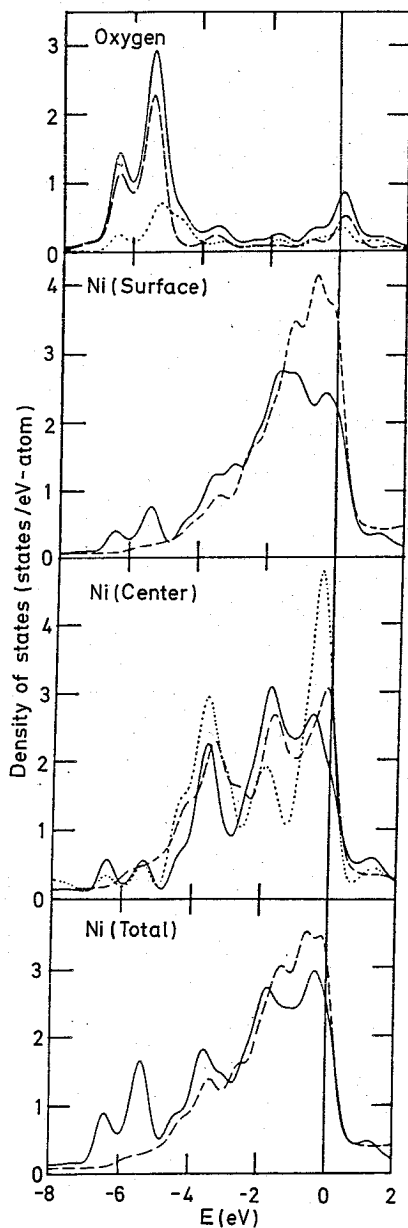


Fig. 13. Total and projected local DOS for three-layer Ni (001) slab (dashed lines) and $c(2 \times 2)$ O on Ni (001) (solid lines) including oxygen e (long dashes) and a_1 (dotted) orbital DOS. Results from ab-initio self-consistent calculations [58].

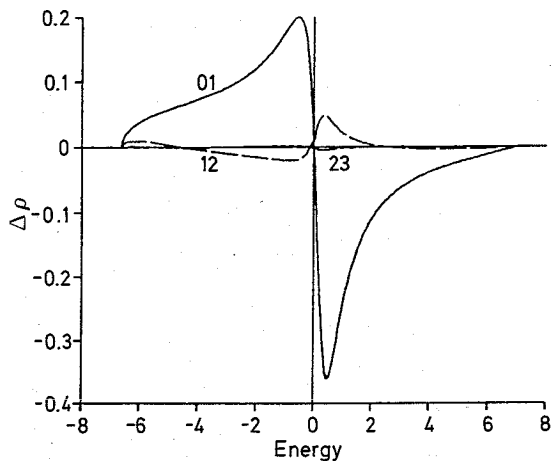


Fig. 14. Bond order electron energy density changes $\Delta\rho_{01}(E)$, $\Delta\rho_{12}(E)$, and $\Delta\rho_{23}(E)$ for the same calculations used to produce results presented in Figs. 11

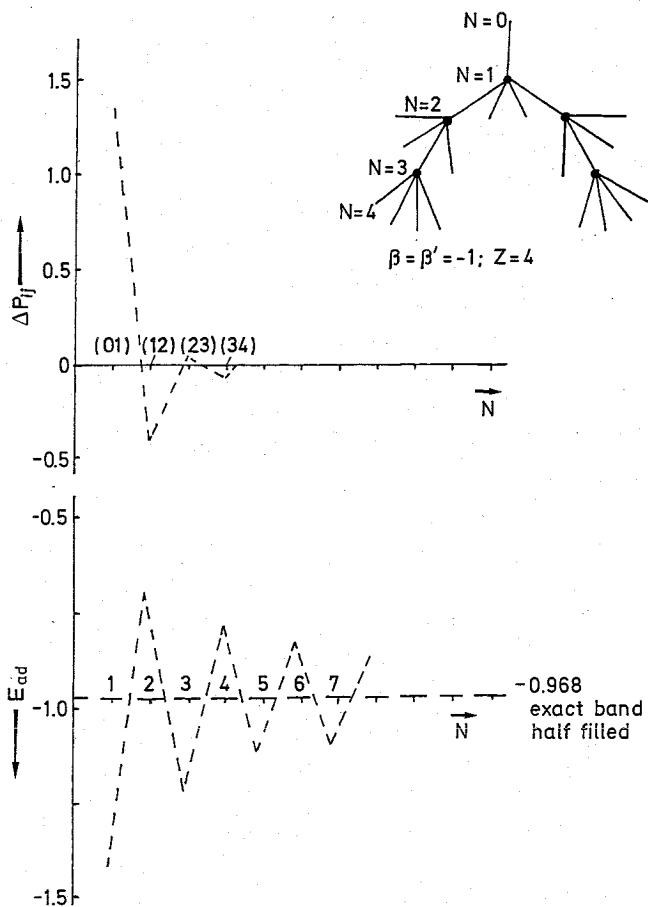


Fig. 15. Changes in bond order and respective energy contributions as a function of distance to adsorbate. For parameters used, see Ref. [55]

there is only an interaction with π type adsorbate orbitals in bridging coordination sites. An increase in bandwidth of the σ electron density of surface atoms occurs if adsorption increases their coordination number. This is a very general phenomenon and follows from (26b). This is illustrated in Fig. 13 for the change in LDOS of surface Ni atoms when O is adsorbed to it according to an ab initio calculation [58].

The changes of the electron density of Ni surface atoms are shown before and after oxygen adsorption. One observes that the bandwidth of electron density on the surface atoms is less than that of the slab center atoms, which relates to the decreased coordination of the surface-atoms compared to the bulk.

Comparison of $\rho_1(E)$ in Fig. 11a and 11b also shows a similar broadening of the LDOS of the surface atom in the Bethe lattice calculations.

Because of conservation of density, broadening of the bandwidth implies that at the center of a band, density decreases in order to balance the increase in density at the edges.

Figure 14 shows the bondorder electronenergydensity $\rho_{01}(E)$ and changes in bondorder electronenergydensities $\Delta\rho_{12}(E)$, and $\Delta\rho_{23}(E)$ from the same Bethe lattice calculation done to produce Figs. 11.

In Figs. 11 and 14, indices refer to the coordination shell with respect to the adsorbed atom.

As expected, $\rho_{01}(E)$ gives a positive bonding contribution at low electron energies, but an antibonding contribution at higher electron energies.

$\Delta\rho_{12}(E)$ the change in bondorder energy density behaves reverse. After adsorption,

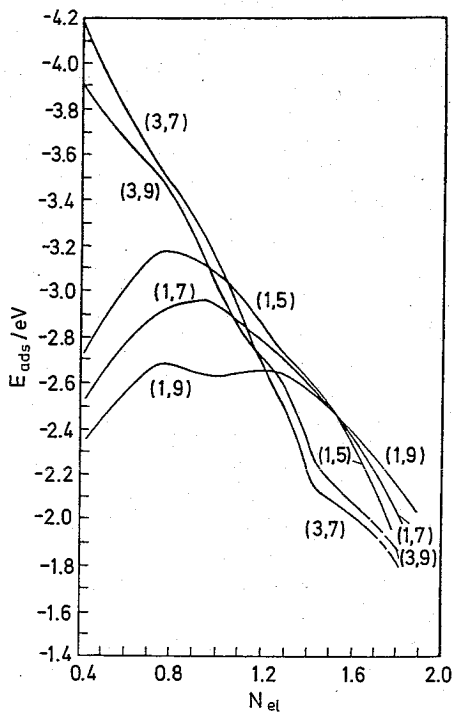


Fig. 16. Interaction energy E_{ads} as a function of N_{el} [51]

there is a decrease of the bonding contribution and increase in the antibonding region, $\Delta\varrho_{23}(E)$ is much smaller, but again shows inverse behavior from $\Delta\varrho_{12}(E)$.

Because of coordination of an hydrogen atom to atom 1, there is a decrease in the bondstrength between atom 1 and those in the second coordination shell if the valence electron band is half filled. Respective contributions to the bond energy ΔE calculated on a Bethe lattice simulating a b.c.c. lattice are given in Fig. 15 for the situation that each metal atom contributes one electron.

One observes that there are still significant contributions to the bond energy 2 or 3 coordination shell distances removed from the adsorbate site.

Whether the bond strength increase with the number of neighbors of the atom concerned depends on the position of the Fermi level with respect to the local density of states maximum and the energy dependence of $\varrho(E)$.

Figure 16 illustrates this by presenting the calculated bondstrengths of an hydrogen-type adsorbate to the (111) face of the f.c.c. s-band model metal as a function of the number of valenceband electrons (N_{e1}). The same Bethe lattice approximation as discussed earlier has been used. As expected, three-coordinated hydrogen bonds more strongly than mono- or dicoordinated hydrogen atoms at low valence-electron

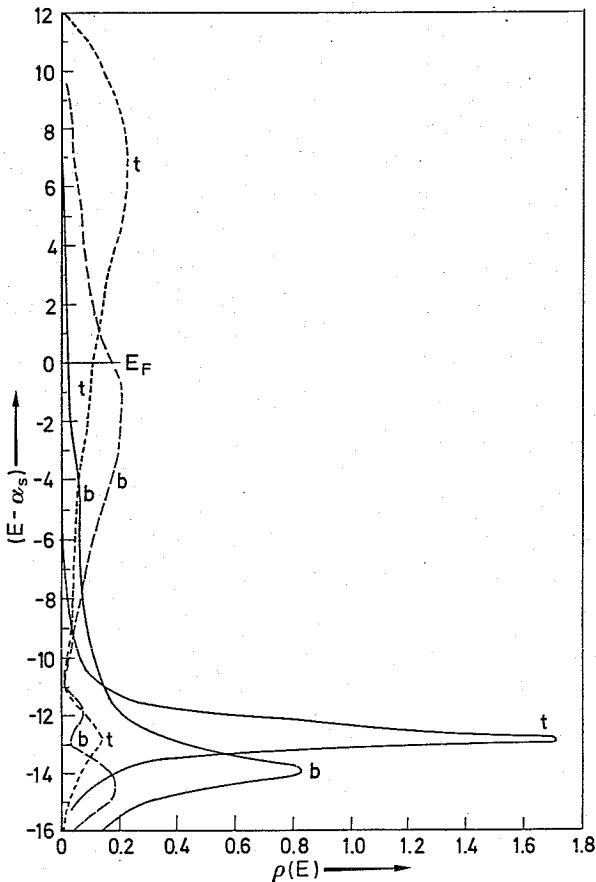


Fig. 17. $\varrho_0(E)$ and $\varrho_{t,b}^s(E)$ for Bethe lattice calculations. $\varrho_{t,b}^s(E)$ are surface group orbital local density of states after chemisorption for atop ($\varrho_t^s(E)$) and three-coordinate ($\varrho_b^s(E)$) adsorption, $\varrho_0(E)$ is the LDOS of the adsorbate orbital. Parameters used are the same as for figure 12.

— $\varrho_0^{(t,b)}$
 - - - $\varrho_{(t,b)}^s$

band filling. This is in line with observations that can be made from Fig. 12. At low valence-electron band filling, more electrons will occupy low energy levels for three-coordinated than for mono-coordinated hydrogen (see also Fig. 17). As a result, according to Eq. (17b), three-coordinated hydrogen is more strongly bonded than monocoordinated hydrogen.

That difference clearly becomes less when the Fermi level increases.

However, the shift from threefold to atop position can only be understood by also considering the LDOS $\rho_i(E)$ of the surface-fragment orbitals that interact with the adsorbed hydrogen atoms. For atop-adsorbed hydrogen, one has to compute the LDOS $\rho_i(E)$ of the atomic orbital ϕ_1 of the metalatom bonded to hydrogen; for three-coordinated hydrogen symmetrically coordinated to three surface metalatoms, it is the LDOS $\rho_i^S(E)$ of the grouporbital $1/\sqrt{3}(\phi_1 + \phi_2 + \phi_3)$.

As is clearly seen in Fig. 17, the metalatom local density of states $\rho_i^S(E)$ is high in the antibonding region; the maximum in local density of states being at higher energy for atop coordination than for threefold coordination. The Fermi level in Fig. 17 is chosen such that the valence-electron band filling of the metal lattice atoms equals one electron per metal atom. One observes that more antibonding levels are occupied for threefold coordination (b) than for atop coordination (c). As a result, atop coordination is more favored.

This illustrates that, in general, bandwidth or bandshifts as measured spectroscopically do not correlate with the bondstrength and that deductions on relative bond energies based on approximations to Eq. (18) have to be considered with care.

A very useful approach to estimate bond energies of adsorbates is to use an extension of frontier orbital theory to chemisorption on metal surfaces [33]. This has been discussed extensively elsewhere, so the basic results will be shortly summarized.

We discussed earlier that orbital overlap causes two effects: Pauli repulsion and reduction of energy dispersion.

Equation (15) will now be replaced by the first- and second-order perturbation approximation to it:

$$E = -4 \sum_{\alpha} \bar{\beta}'_{\alpha} S_{\alpha} - 2 \left\{ \sum_{\substack{\alpha, i \\ E_i > E_F \\ E_{\alpha} \text{ occ}}} |\bar{\beta}'_{\alpha i}|^2 \frac{1}{E_i - E_{\alpha}} + \sum_{\substack{\beta, j \\ E_j < E_F \\ E_{\beta} \text{ unocc}}} |\bar{\beta}'_{\beta j}|^2 \frac{1}{E_{\beta} - E_j} \right\} \quad (24)$$

The first term represents the Pauli repulsion between the fragment orbitals that are allowed to interact. These are sketched in Fig. 18.

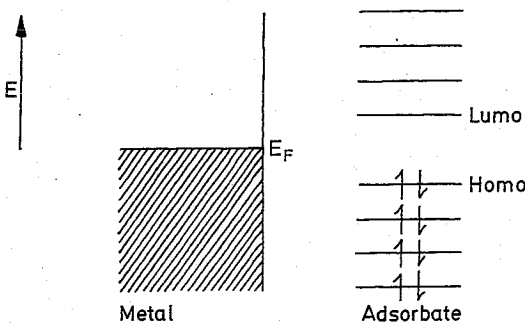


Fig. 18. Schematic illustration of relative position of adsorbate and metal surface orbitals

E_α are the highest occupied molecular orbitals (HOMO) of the adsorbate, E_β are the lowest unoccupied molecular orbitals (LUMO) of the adsorbate, E_i the metal LUMOs, and E_j the metal surface HOMOs.

The second term of Eq. (24) represents electron backdonation from adsorbate to surface, the third electron back donation from metal surface to adsorbate.

The attractive part of Eq. (24) can be partially integrated to give Eq. (25):

$$E_{\text{attr}} = -2 \left\{ \sum_{\alpha} \varrho_{\alpha}(E_F) \bar{\beta}'_{\alpha}{}^2 \frac{\Delta_{\alpha} \cdot (1 - P_{\alpha})}{- \phi - \frac{e^2}{r_{\alpha} + k_{\alpha}} - E_{\alpha} + \Delta_{\alpha} \cdot (1 - P_{\alpha})} + \sum_{\beta} \varrho_{\beta}(E_F) \bar{\beta}'_{\beta}{}^2 \frac{\Delta_{\beta} \cdot P_{\beta}}{E_{\beta} - \frac{e^2}{4r_{\beta} + k_{\beta}} + \phi + \Delta_{\beta} \cdot P_{\beta}} \right\} \quad (25)$$

$\varrho_{\alpha}(E_F)$ is the group-orbital electron density at the Fermi-level energy [59, 60, 61]:

$$\varrho_{\alpha}(E_F) = \sum_i |\langle \varphi_{\alpha} | \psi_i \rangle|^2 \delta(E_F - E_i)$$

φ_{α} is a linear combination of surface atomic orbitals, ψ_i a metal surface orbital eigenfunction with corresponding energy E_i .

$$\bar{\beta}'_{\alpha} = \langle \chi_{\alpha} | \bar{H}' | \varphi_{\alpha} \rangle \quad (26)$$

and

$$S_{\alpha} = \langle \chi_{\alpha} | \varphi_{\alpha} \rangle \quad (27)$$

For s-type orbitals:

$$\beta' \sim Z'^{1/2} \beta'_0 \quad (28a)$$

β'_0 is the overlap energy integral found for atop adsorption, and

$$S_{\alpha} \sim Z'^{1/2} S_0 \quad (28b)$$

S_0 is the overlap integral found for atop adsorption, with Z' the number of neighbors of the adsorbate orbital. Since H' is totally symmetric, χ_{α} (the adsorbate molecular orbital) determines the symmetry of the surface metal-orbital fragment φ_{α} , which is the group orbital.

Δ_{α} is the total bandwidth of the metal valence-electron band corresponding to φ_{α} , and P_{α} is a measure of the electron occupation of that electron band.

$$P_{\alpha} = E_F / \Delta_{\alpha} \quad (29)$$

$-\Phi$ is the work function of the metal surface considered, and the term $-e^2/(4r_{\alpha} + k_{\alpha})$ represents the image potential interaction of ion state α , with effective adsorbate to metal distance r_{α} and screening k_{α} [6].

Equation (25) relates the attractive component of the binding energy to:

- the group orbital local density of states at the surface metal Fermi level,
- the effective energy difference between adsorbate orbitals and the Fermi level,
- the surface metal orbital electron occupation,
- orbital overlap.

This is a remarkable result. Whereas it has been suspected by many authors (see Grimely [62]) that a relation between bondstrength and local density of states at the Fermi level should exist, Eq. (25) states this relation with the modification that the grouporbital local of states should be used. Others [63] have derived related expressions, but ignored the $\rho(E_F)$ term. Falicov and Somorjai [64] propose to correlate catalytic activity with low-energy local electronic fluctuations in transition metals.

Electronic fluctuations are well known to be related to the local electron density of states at the Fermi levels and the occupied and unoccupied fraction of the valence-electron bands.

Equation (24) appears to quantify this and modifies the importance of the local density of states to that of the grouporbital density of states at the Fermi level.

Figure 19 shows the LDOS of different grouporbitals of the s-electron band for the (111)-face of a f.c.c. crystal calculated in the Bethe lattice approximation.

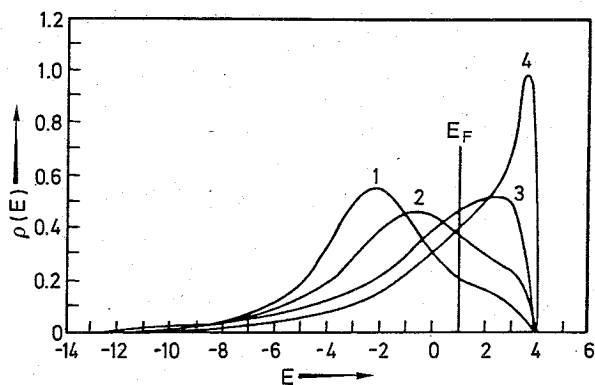


Fig. 19. LDOS $\rho_i(E)$ of different group orbitals of the electron band for a (111) face of a f.c.c. crystal calculated in the Bethe lattice approximation [51]
 $i = 1$ σ three coordination; $i = 2$ σ two coordination; $i = 3$ σ atop coordination; $i = 4$ π two coordination

It is observed that at an electron occupation number of one electron per atom and for an adsorbate orbital of σ symmetry:

$$\rho_{\text{atop}}(E_F) > \rho_{\text{bridge}}(E_F)$$

Hence, at this electron bandfilling, already atop adsorption becomes favored as can be seen by comparison with the bond energies presented in Fig. 16.

In agreement with the results discussed earlier at lower band filling, the higher-coordinated hydrogen atoms become more stabilized because of the relative increase in grouporbital local density of states.

3 Bonding to Metal Clusters

In this chapter, the results of ab-initio calculations will be analyzed within the extended Hückel theory conceptual framework. This provides also an opportunity to discuss explicitly effects due to the orbital symmetry of the fragments. The differences in chemical bonding to small and large clusters will be considered here. In the last chapter, the analysis will be extended to semi-infinite lattices. We will discuss studies of H_2 dissociation extensively and comment shortly on the reactivity of methane and ethane. For comparison, also a discussion of CO chemisorption will be presented.

3.1 Chemisorption and Dissociation (Oxidative Addition) of H_2 to Transition Metal Atoms

Extensive ab-initio calculations on oxidative addition to bare and complexed atoms have appeared during the past years.

Here, we mainly discuss the work of the Siegbahn group [64, 66] and the group of Goddard [66, 67] and Nakarsuji [68]. Other important studies have been done by Kitaura et al. [69] and Noell and Hay [70]. The work up to 1985 has been excellently reviewed by Dedieu [71]. The elementary interactions playing a role in oxidative addition have been recently analyzed by JT Saillard and R Hoffmann [47], who also compared H_2 dissociation on single metal atom clusters and metal surfaces.

Three main effects play a role:

As expected on the basis of frontier orbital theory, the *symmetries* of highest occupied molecular orbitals (HOMO) on the one fragment, and empty lowest unoccupied molecular orbitals (LUMO) on the other fragment and vice versa have to match. Sometimes they do not match. By *promotion* of electrons in a fragment to unoccupied orbitals, orbitals of proper symmetry may become available. The required promotion energy is paid back by the resulting increase in bond energy. *Hybridization* of the orbitals to allow for optimum overlap is the third factor of importance. Hybridization of the orbitals in order to optimize overlap in particular directions also requires promotion of electrons, so promotion and hybridization are closely interconnected. Such effects are very general. We will discuss them here for H_2 dissociation as well as for CO chemisorption. Adsorption and dissociation of H_2 to a Ni atom has been thoroughly studied by Blomberg and Siegbahn [64] using CASSCF (complete active space SCF) and contracted CI calculations. The results are summarized in Fig. 20. The calculated ground state of Ni is $3d^8 4s^2$ with the spins in a triplet state (experimentally the $^1D(d^9s^1)$ state is 0.03 eV lower). The H_2 molecule approaches the Ni atom symmetrically.

Because of the small overlap, the triplet state Ni 3d electrons interact only weakly with H_2 . The doubly occupied Ni 4s orbital has a repulsive interaction with the doubly occupied H_2 σ orbital, so bond formation is symmetry-forbidden. This results in a large activation energy for hydrogen addition (38 kcal/mole). In NiH_2 , the angle ϕ between the NiH bonds is 180° , agreeing with sp hybridization between the doubly occupied 4s and empty 4p orbital of Ni. Addition of H_2 appears to be energetically neutral. The activation energy for H_2 addition becomes significantly decreased if

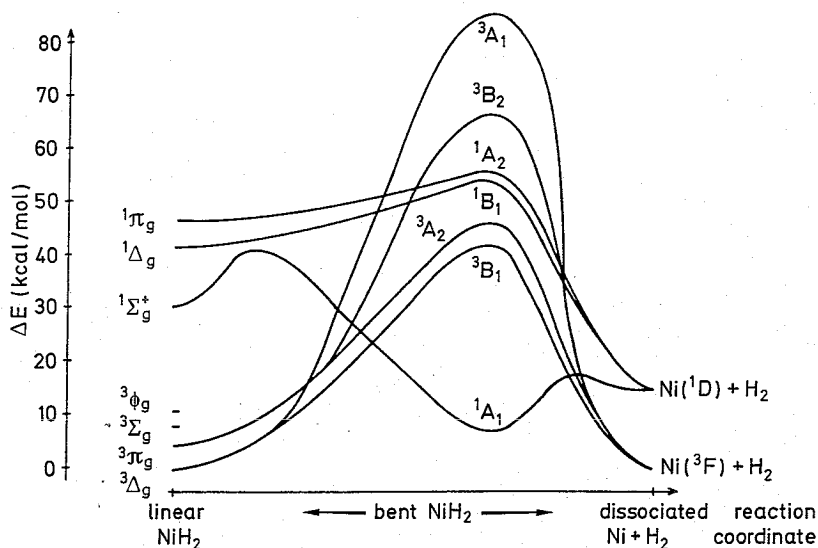


Fig. 20. Dissociation curves for triplet and singlet states of NiH_2 . The energies are relative to H_2 and the ^3F state of nickel [64]

promotion of electrons from 4s to 3d orbitals can occur. The promotion energy cost is 15 kcal/mol, but reaction between the $\text{Ni } d^9s^1$ (^1D) and H_2 is now symmetry-allowed. Electrons can be donated from the doubly occupied H_2 σ orbital into the now partially occupied $\text{Ni } 4s$ orbital and an antisymmetric $\text{Ni } d$ orbital can backdonate into the empty H_2 σ^* orbital. As a result, the overall activation energy for H_2 addition decreases to 15 kcal/mol and an endothermic quasi-stable $^1\text{A}_1$ NiH_2 state is found to exist at an energy of 8 kcal/mol above the triplet state. The configuration of the $^1\text{A}_1$ NiH_2 state is now bent, with an angle ϕ equal to 50° . The $^1\text{A}_1$ state can be approximately described as a Ni atom in the d^9 state and hybridization between d_{xy} and s orbital (Fig. 21). The predicted angle would however be 90° , indicating that the H_2 molecule has not yet completely dissociated. It should be noted that H_2 readily dissociates on a Ni metal surface, without any activation energy. The reason for this difference will be discussed later.

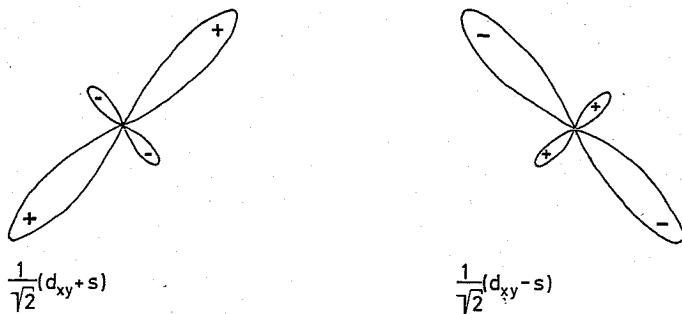


Fig. 21. Hybridized d_{xy} and s orbitals

Addition of H_2 to Pd and a $Pd(H_2O)_2$ complex using similar methods has been studied by UB Brandemark et al. [65]. Table 2 [65] summarizes their results. This study demonstrates the importance of prehybridization by the presence of ligands. We first consider addition to the Pd atom. Promotion of the Pd atom $4d^{10}$ state to a $4d^9s^1$ state is calculated to cost 40 kcal/mol. The ground state of Pd is $4d^{10}$. So, if only the 4d orbital is involved, symmetrical addition of H_2 is symmetry-forbidden, similarly to Ni in the d^8s^2 state.

Table 2. Geometries and energies for PdH_2 and $(H_2O)_2 PdH_2$ [65]

Geometry	$R(Pd-H)$	θ	$R(Pd-HH)$	$R(H-H)$	$R(Pd-O)$	ϕ	rel energy
Asymptote ($Pd + H_2$)	∞		∞	1.40			0
PdH_2	3.65	23	3.58	1.46			-5.5
Asymptote $((H_2O)_2Pd(\text{linear}) + H_2)$	∞		∞	1.40	4.40	180	0
Asymptote $((H_2O)_2Pd(\text{bent}) + H_2)$	∞		∞	1.40	4.40	90	15.0
PdH_2 geometry	3.65	23	3.58	1.46	4.40	90	-2.0
Equilibrium	2.89	65	2.43	3.14	4.40	90	-6.9

Distances in au and angles in degrees. Energies in kcal/mol.

H_2 addition to Pd is exothermic by -5.5 kcal/mol.

(Using SAC and SAC-CI methods, Nakatsuji et al. [68] report a value of 15 kcal/mol indicating perhaps that the energy differences calculated are more comparative than quantitative). The angle ϕ between the two PdH bonds equals 23° and H_2 is not dissociated. Bonding occurs because of donation of electrons from the H_2 σ orbital into the empty Pd 5s orbital and backdonation from an antisymmetric Pd 4d orbital into the antibonding H_2 σ^* orbital. The Pd configuration remains, however, close to $Pd d^{10}$. The calculations on $Pd(H_2O)_2$ were done with an angle of 90° between the H_2O molecules. The important characteristic of the H_2O ligands (and the PR_3 ligands to be discussed below) is the presence of a low-lying occupied σ (lone-pair donor) orbital. The d_{xy} orbital mixes into the antisymmetric combination of these σ ligand orbitals in a bonding (stabilizing) fashion, and is itself destabilized by antibonding interaction. The antibonding interaction with the σ lone pairs is alleviated by admixture of a 5 p_y Pd orbital which has the effect of hybridizing the d_{xy} away from the σ lone pairs and towards the vacant coordination site. The 5s is less destabilized by interaction with the symmetry combination of the H_2O lone-pair orbitals. It leads to bonding and antibonding combinations of H_2O σ orbitals with the $\frac{1}{\sqrt{2}}(d_{xy} + s)$ and $\frac{1}{\sqrt{2}}(d_{xy} - s)$ hybridized orbitals of Pd. As a consequence, the promotion energy from the $4d^{10}$ configuration is lowered. The computed difference between the $^1S(d^{10})$ and $^1D(d^9s^1)$ state is now only 20.4 kcal/mol instead of 40 kcal/mol found for the bare Pd atom. As a result, the H_2 molecule can dissociate when reacted with $Pd(H_2O)_2$. The resulting angle ϕ between the PdH atoms is found to be 65° and the dissociation energy as -6.0 kcal/mol, with respect to linear $Pd(H_2O)_2$. The difference in energy

between bent and linear $\text{Pd}(\text{H}_2\text{O})_2$ is 14 kcal/mol, linear $\text{Pd}(\text{H}_2\text{O})_2$ being more stable. Its electronic structure is very similar to that of the linear $\text{Pt}(\text{PH}_3)_2$ to be discussed later. Addition of H_2 is accompanied by moving the H_2O molecules from the linear to bent configurations. In this process, the Pd atom becomes excited to the d^9 configuration.

This demonstrates that ligand addition to an atom may increase the interaction energy with a reacting fragment. The ligands promote electrons in the complex for optimal bonding. Vacant hybridized orbitals become directed towards empty ligand position(s).

As will be shown later, similar effects also occur on surfaces, explaining partly the changed reactivity of surface atoms compared to free atoms [33].

Low and Goddard [66, 67] also studied the interaction of H_2 , methane, and ethane with Pd and the interaction of H_2 with the $\text{Pt}(\text{PH}_3)_2$ complex using ab-initio methods.

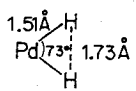
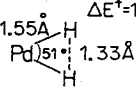
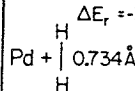
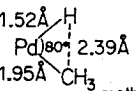
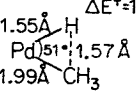
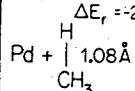
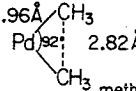
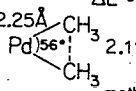
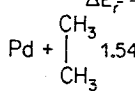
Representative results for Pd and Pt are presented in Figs. 22 and 23 resp. Starting with dissociated H_2 , CH_4 , and C_2H_6 on Pd (not stable according to Blomberg et al. [64]), they calculate the activation energies for dissociation. They find an increasing barrier for reductive elimination moving from H_2 to CH_4 to C_2H_6 .

The orbital density plots show the hybridized nature of the bonding Pd atom orbitals. Reaction of H_2 with the $\text{Pt}(\text{PH}_3)_2$ complex is very similar as that with $\text{Pd}(\text{H}_2\text{O})_2$. As in the case of $\text{Pd}(\text{H}_2\text{O})_2$ the free $\text{Pt}(\text{PH}_3)_2$ molecule is linear. Whereas the groundstate of Pt is $5d^9 6s^1$, the Pt d orbital occupation in $\text{Pt}(\text{PH}_3)_2$ is $5d^{10}$. This is because the doubly occupied phosphine σ orbitals form bonding as well as antibonding orbitals with sp hybrids. The four phosphine electrons are accommodated in the bonding orbitals, the single s electron is placed in a low d orbital rather than in an antibonding ligand-metal (sp) orbital. An alternative way of viewing this process is that promotion of the 6s electron into the 5d orbital of Pt reduces the repulsive interaction between the two doubly occupied phosphine orbitals and the Pt s orbital. Oxidative addition of H_2 decreases the angle between the phosphine groups to 100° , enabling hybridization of the Pt 6s and $5d_{xy}$ orbital with a resulting angle between the PtH bonds of 80° . This is very similar to bonding to the bent $\text{Pd}(\text{H}_2\text{O})_2$ complex. The activation energy to dissociation is 2.34 kcal/mol, the dissociation energy of 18 kcal/mol is exothermic. Noell and Hay report similar but quantitatively different results [70]. The same holds for the work by Kitaura et al. [69]. (cf., the comparison made by Dedieu [71]).

Again we observe the favorable effect of surrounding the reacting metal atom with ligands. Now, the rotated PH_3 groups prepromote the electrons in Pt so as to give hybridized orbitals of favorable orientation.

Bonding with a Pt atom complex exceeds that with Pd because of the spatial extension of the Pt orbitals. Compare the respective bond energies of the hydrides ($\text{PtH} = 83$ kcal/mol, $\text{PdH} = 76$ kcal/mol, $\text{NiH} = 60$ kcal/mol) [69].

Figure 23 shows the computed generalized valence-bond (GVB) orbitals for the $\text{H}_2\text{Pt}(\text{PH}_3)_2$ complex. Figure 23b shows the GVB orbitals in PtH. Note that the 6p orbitals do not participate in the PtH bond, which can be considered as a linear combination of a hybridized $\text{Pt}(5d_{z^2}, 6s)$ bond and $\text{H}(s)$ orbital, but they do participate in the Pt-H bonds in $\text{H}_2\text{Pt}(\text{PH}_3)_2$. The picture that derives for bonding to the last members of the transition-metal series in the periodic system is very clear. Upon dissociation of H_2 , localized bonds are formed between two (s, d_{xy}) metal orbitals

Reactants	Transition State	Products
0 kcal/mol 	$\Delta E^\ddagger = 1.55 \text{ kcal/mol}$ 	$\Delta E_r = -3.55 \text{ kcal/mol}$ 
0 kcal/mol 	$\Delta E^\ddagger = 10.4 \text{ kcal/mol}$ 	$\Delta E_r = -20.1 \text{ kcal/mol}$ 
0 kcal/mol 	$\Delta E^\ddagger = 22.6 \text{ kcal/mol}$ 	$\Delta E_r = -15.95 \text{ kcal/mol}$ 

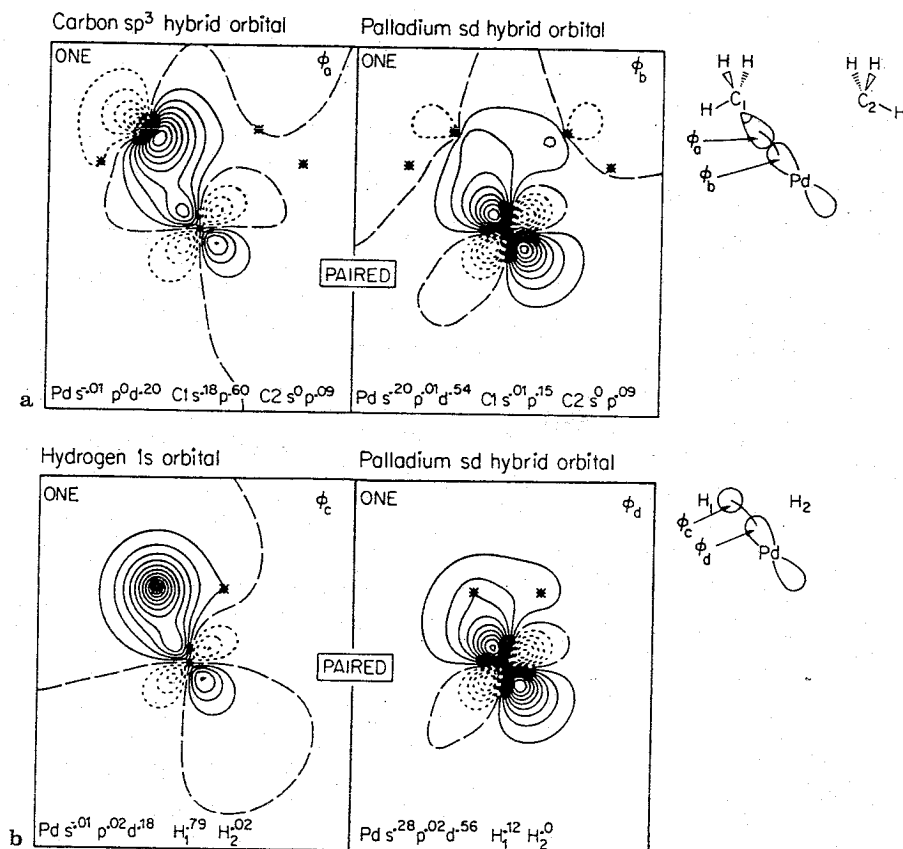
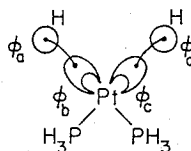
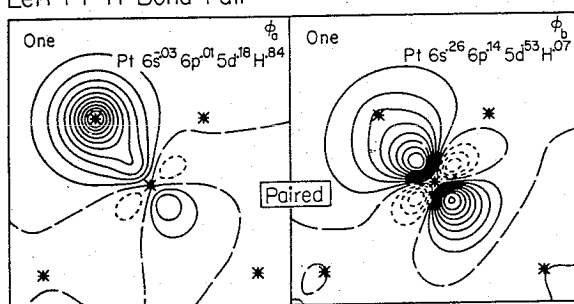


Fig. 22a. Geometries and energetics for the reactions $\text{PdH}_2 \rightarrow \text{Pd} + \text{H}_2$, $\text{PdH}(\text{CH}_3) \rightarrow \text{Pd} + \text{CH}_4$, and $\text{Pd}(\text{CH}_3)_2 \rightarrow \text{Pd} + \text{C}_2\text{H}_6$. The angle between the Pd-C bond and the vector from the C atom to the center of mass of the methyl hydrogen atoms is defined to be the methyl tilt [67]; b GVB orbital for the Pd-C bonds at the transition state for the reaction $\text{Pd}(\text{CH}_3)_2 \rightarrow \text{Pd} + \text{C}_2\text{H}_6$ and the GVB orbitals for the PdH bond for the reaction $\text{PdH}_2 \rightarrow \text{Pd} + \text{H}_2$. The Mulliken populations are listed with each orbital to show the hybridization of each orbital [67]

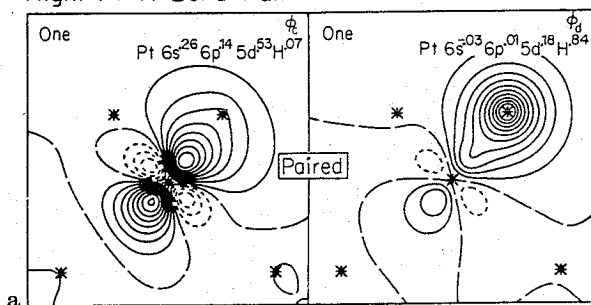
and the hydrogen atom orbitals, resulting in orbital energies low compared to the d-atomic orbitals (Fig. 24b).

The theoretical angle between the M-H bonds is 90° and two electrons reside in each of the bonding M-H orbitals. The bondstrength of a M-H bond is large, between 80 and 60 kcal/H atom and decreases from Pt to Pd to Ni. The metal atom part not involved in bonding is in a M^{2+} state, in line with the notion of oxidative addition

Left Pt-H Bond Pair



Right Pt-H Bond Pair



Pt 6s-5d hybrid orbital Hydrogen orbital

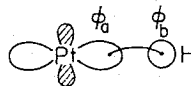
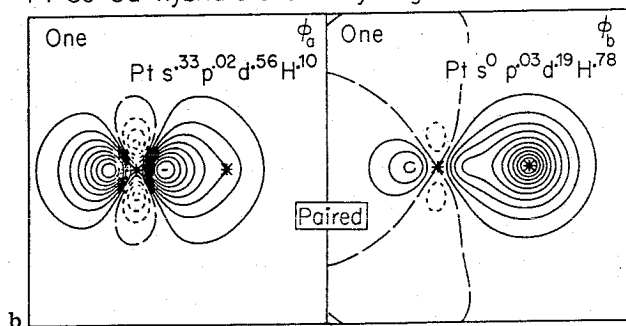


Fig. 23a. GVB orbitals for the Pt-H bonds of $H_2 Pt(CH_3)_2$ at equilibrium. Hybridization for each singly occupied GVB orbital is shown on each plot. Each contour represents a change of 0.05 in amplitude. Solid lines represent positive amplitude. Asterisks represent positions of atoms [66]; **b** GVB orbitals for diatomic PtH [66]

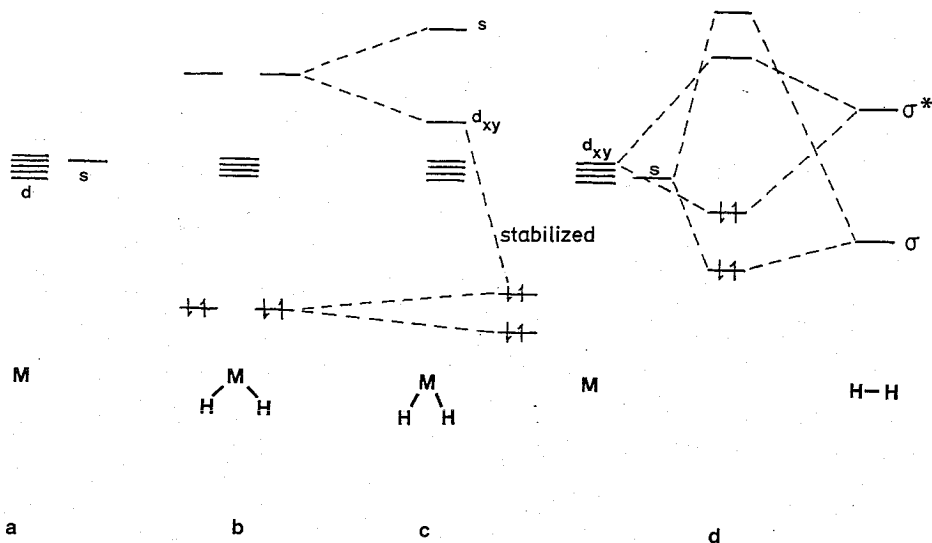


Fig. 24a-d. Schematic electronic orbital scheme of reductive elimination. **a.** Orbital levels of free metal atom. **b.** Dissociated H₂ bonded to a metal atom (hybridization of s and d_{xy} orbital), $\varphi = 90^\circ$. **c.** Reductive elimination; $\varphi < 90^\circ$. **d.** Oxidative addition; σ and σ^* are, respectively, bonding and antibonding H₂ orbitals

commonly applied to dissociative adsorption of H₂ to a transition-metal atom complex.

Berke and Hoffmann [72] have given a very illuminating picture of the events and orbital symmetry constraints that govern reductive elimination and oxidative addition.

We will illustrate this for hydrogen recombination starting with an initial configuration where the M-H bonds have an angle of 90°. Suppose ideal d_{xy} and s hybridization on the metal atom. If the angle between the M-H bonds decreases, the initially nearly degenerate bonding and antibonding orbitals of the two bonds interact and four new orbitals result (see Fig. 24c). Bonding and antibonding combinations of the bonding M-H orbitals and the analogous combination for the antibonding M-H orbitals are formed. The energy change will be repulsive upon decreasing the angle, because bonding as well as antibonding orbitals become doubly occupied. This repulsive interaction is decreased if electrons are transferred from the doubly occupied antibonding combination of M-H bonds to unoccupied metal orbitals. Or in other words, the energy of the antibonding orbitals is decreased because of interaction with an unoccupied d orbital of proper symmetry. Decreasing the angle ϕ between the M-H bonds changes the hybridization of the metal orbital part of the M-H bond. So at an angle $\phi < 90^\circ$, the orbital scheme becomes as sketched in Fig. (24c). An empty d orbital of d_{xy} symmetry is required on the metal atom. In summary apart from this orbital three orbitals are of importance in the recombination of the hydrogen atoms: a symmetric low-lying orbital leading to the bonding H₂ σ orbital, an antisymmetric doubly occupied orbital leading to the σ^* orbital of H₂, and an s-type metal orbital that is pushed away to high energy. The antisymmetric orbital is initially

occupied and results in repulsion with decreasing angle ϕ . The energy of the anti-symmetric orbital is decreased if it can interact with a suitable d-orbital of the same symmetry. Whether such an orbital is empty and energetically available usually depends on the ligand configuration around the metal atom and the metal atom electron occupation. In our case of a free metal atom, such an orbital is provided by the d_{xy} orbital. As a result, when the hydrogen atom distance decreases, more electrons are donated in the empty d-orbital and at infinite distance from each other, a neutral metal atom and H_2 molecular appear (reductive elimination).

The increased activation energies found for the reductive elimination of methane and ethane derive from additional repulsive interactions between doubly occupied bonding C-H bonds with the M-H bond or the C-H bond of the molecule fragment. Such repulsive effects have also been described by Zheng, Apelaig and Hoffmann [73] between methyl hydrogen atoms and surface metal atoms.

3.2 Reaction of H_2 with Transition Metal Clusters

A recent ab-initio study of H_2 dissociation on Pd_2 [68] and an older study on the reaction of H_2 on Ni exist [74]. Addition of H_2 in a symmetrical way parallel to the metal dimer is considered. Compared to bonding to a metal atom, the main additional feature of a dimer is that antibonding combinations of occupied s or d orbitals on the different atoms, if occupied by electrons, provide additional possibilities for interaction with unoccupied orbitals of π symmetry and that dissociated atoms can bind to different metal atoms.

Nakatsuji et al. [68] report a complexation energy of -12 kcal/mol and an H-H distance of 0.9 \AA and a Pd-Pd distance equal to 2.8 \AA for H_2 to Pd_2 using the CAS-MS-SCF method. An adsorption energy of -15 kcal/mol for H_2 molecule complexation to a Pd atom and a PdH bond strength of 54 kcal/mol is calculated by the same method. Upon dissociation, an activation energy of 3.4 kcal/mol and

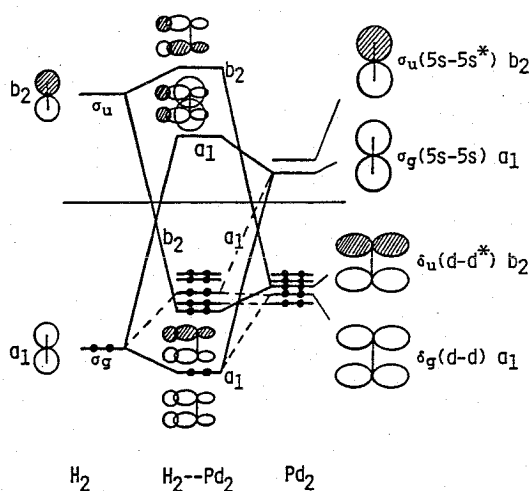


Fig. 25. Schematic correlation diagram for the interaction of H_2 and Pd_2 [68]

an additional energy gain of -2.2 kcal/mol is found, implying a PdH bond strength of 59 kcal/gat H. The H-H distance after dissociation becomes 2.1 Å. According to this calculation, first a precursor state of molecular H_2 is formed that consecutively converts to dissociated hydrogen, with each hydrogen atom attached to a different Pd atom. Bonding in the Pd_2H_2 molecule is schematically sketched in Fig. 25. In the Pd_2 molecule, the bonding as well as antibonding s orbitals are unoccupied and the symmetric as well as antisymmetric d-orbital combinations are occupied (implying weak bonding in the Pd_2 molecule, $E_{diss}^{exp} = 17$ kcal/mol).

According to HOMO-LUMO considerations, addition of H_2 to Pd_2 is clearly symmetry-allowed. As a result, exothermic dissociation of H_2 on Pd_2 becomes possible, whereas on an isolated Pd atom the dissociation reaction does not occur.

Bonding of Pd atoms in a dimer has decreased the promotion energy from 4d to 5s which is the cause of the strong repulsion of H_2 with the Pd atom.

Whereas no calculation of dissociation of H_2 on Cu_2 is available, clearly dissociation as well as addition of the hydrogen molecule becomes symmetry-forbidden. The a_1 orbital that consists of the symmetrical combination of metal s orbitals, empty in Pd_2 , becomes occupied in Cu_2 .

We will return to the reactivity of Cu_2 in a discussion of the reactivity of Co. Melius et al. [74] studied dissociation of H_2 parallel to the Ni_2 dimer.

The major difference between Ni_2 and Pd_2 is that in Ni_2 the d valence orbitals remain partly empty. Therefore, in Ni_2 the bonding orbital formed from the two

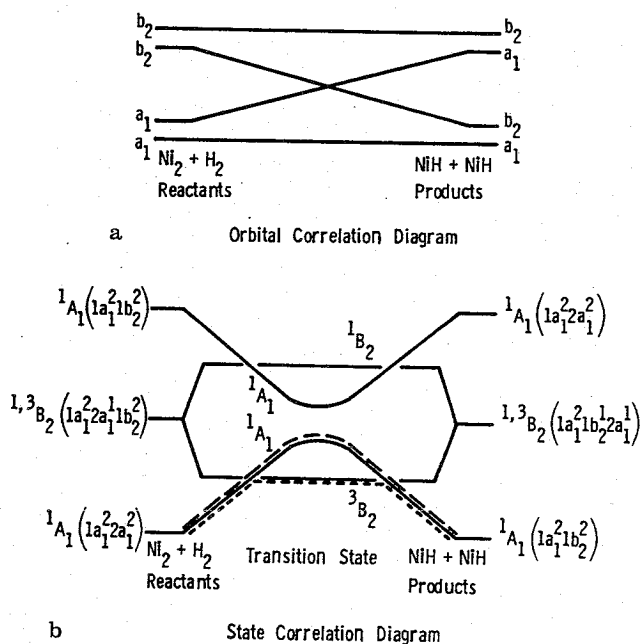


Fig. 26a and b. Orbital and state correlation diagrams for the reaction $H_2 + Ni_2 \rightarrow 2 NiH$. The long-dashed curve indicates the reaction path for which the valence symmetry is conserved. The short-dashed curve indicates the reaction path for which the valence symmetry changes (${}^1A_1 \rightarrow {}^3B_2 \rightarrow {}^1A_1$) [74]

Ni 4s atomic orbitals is occupied. Ignoring the interaction with the Ni d orbitals, the dissociation reaction of H_2 to Ni_2 would be clearly Woodward-Hoffmann-forbidden and a large activation energy for dissociation is expected. The orbital and state correlation diagrams for the dissociation reaction is given in Fig. 26. Total energies are given in Table 3. As observed, the calculated activation energy is 21 kcal/mol, which is comparable to that found for the Ni atom.

Table 3. Ni_2H_2 energies [74]

Method	State	R_1 (0.74 Å)	R_2 (1.06 Å)	R_3 (2.49 Å)
HF (1 cf)	1A_1	0.0 ^a	1.57	0.15
HF (1 cf)	3B_2	-0.73	0.03	1.80
MCSCF (12 cf)	1A_1	0.0 ^a	0.96	0.18
MCSCF (8 cf)	3B_2	0.09	0.69	2.49

^a Reference point energy has been set equal to zero. The total energy of the 1A_1 state at R_1 is -39.33 eV (HF) and -40.66 eV (MCSCF).

Siegbahn et al. [75] studied H_2 dissociation on a Ni_{13} cluster simulating the Ni(100) face using similar techniques as applied to the NiH_2 systems discussed earlier. However, to make the computational problem tractable, in some cases modified effective core potentials (MEP) had to be used excluding 3d orbitals to take part in the dissociation process. Dissociation atop of a Ni atom was, however, calculated without restricting the degree of freedom corresponding to that of the Ni 3d atom electrons. Dissociation in a bridging configuration again could only be done with frozen 3d electrons.

Table 4a shows for atop dissociation that in order to lower the activation energy for dissociation, covalent interaction with the transition-metal d electrons is a necessity. This indicates the importance of the metal to adsorbate backdonation interaction involving the unoccupied H_2 σ^* level. Since s orbitals are totally symmetric, only interaction with d orbitals can provide this stabilizing interaction. If d electrons are not allowed to interact, an activation energy of 48 kcal/mol is calculated. The interaction with the d electrons lowers the activation energy for dissociation to 4–5 kcal/mol, which compares with 15 kcal/mol for the isolated Ni atom. Whereas no complete dissociation occurs on a Ni atom and H_2 addition is thermodynamically neutral, on the Ni cluster H_2 dissociates exothermally with a dissociation energy of 2 kcal/mole.

Note that in contrast to the activation energy, the interaction with the d electrons is not essential to compute proper values for the Ni–H interaction, resulting in Ni–H bonds of 53 kcal/gat, which is close to the experimental value.

This agrees with our conclusions [37] based on an analysis of experimental data, and those of Upton and Goddard [76] to be discussed later.

MEP calculation with frozen d orbitals results in an activation energy of 28.5 kcal/mol for H_2 dissociation in a bridging configuration (Table 4b). This

compares with 48 kcal/mol for atop dissociation using the same frozen d-orbital approximation.

The difference derives because in the bridge site of the Ni_{13} cluster backdonation of electrons into the antibonding σ^* H_2 level becomes possible by interaction with a populated antisymmetric combination of 4s Ni atom orbitals. In the bridging configuration, antisymmetric 4s Ni atomic orbital combinations become populated.

Table 4a. Reaction energies (kcal/mol) and geometries for on-top dissociation of H_2 on Ni_{13} [75]

Energetics							
	Transition state		SCF	Adsorbed			
	SCF	CI ^a		CI ^a	CI ^a		
12 MEP	66.4	4.4(17.0)	29.2		-2.0(10.5)		
All MEP	57.3	48.0(50.3)	-4.7		-3.8(-4.5)		
Geometries							
	R_1	Transition state				Adsorbed	
		SCF	CI	$R_{\text{H-H}}$		SCF	$R_{\text{Ni-H}}$
12 MEP	2.66	2.51	1.95	2.37	2.83	2.78	
All MEP	2.53	2.53	2.47	2.55	2.82	2.83	
	R_1	Adsorbed				Adsorbed	
		SCF	CI	$R_{\text{H-H}}$		SCF	$R_{\text{Ni-H}}$
12 MEP	2.04	2.07	4.51	3.89	3.04	2.84	
All MEP	1.91	1.92	4.87	4.88	3.10	3.10	

^a Values within parentheses do not contain Davidson's correction

Table 4b. Reaction energies and geometries of the bridge site dissociation of H_2 toward the on-top site on Ni_{14} [75]

Energetic							
All MEP	Transition state				Adsorbed		
	SCF	CI ^a	CI ^a		SCF	CI ^a	
	4.10	28.5(31.6)			-32.8	-33.8(-33.8)	
Geometries							
All MEP	R_1	Transition state				Adsorbed	
		SCF	CI	$R_{\text{H-H}}$		SCF	$R_{\text{Ni-H}}$
	2.77	2.79	2.70	2.79	2.95	2.95	
All MEP	R_1	Adsorbed				Adsorbed	
		SCF	CI	$R_{\text{H-H}}^b$		SCF	$R_{\text{Ni-H}}$
	1.92	1.92	4.71	4.71	3.10	3.10	

^a Values within parentheses do not contain Davidson's correction

^b The $R_{\text{H-H}}$ was not optimized; the H's were positioned at the bridge site

These are empty for the Ni₂ molecule, but in the Ni₁₃ cluster they become partially occupied because of the interaction with the s orbitals of the surrounding Ni atoms.

The dissociation energy for H₂ dissociation resulting in two H atoms sharing the same Ni atom is -2 kcal/mol. If no Ni atoms are shared, the dissociated energy increases significantly to -34 kcal/mol, because now the unfavorable interaction between two Ni-H bonds on the same Ni atom is absent.

Upton and Goddard [76] studied hydrogen-atom adsorption to Ni₂₀ and Ni₂₈ atom clusters, also in the MEP approximation for the Ni 3d electrons.

We will discuss their results for Ni₂₀ clusters.

These results are very relevant also to our discussion of the interaction of adsorbing molecules to semi-infinite metal lattices. Table 5 shows bond strengths and frequencies as a function of hydrogen-atom coordination. One observes increases in bond strength with hydrogen coordination number. Secondly, bonding is strongest to those nickel atoms that have the largest number of nickel metal atom neighbors. The last result is unexpected. Since delocalization of electrons is expected to increase with increasing number of metal atom neighbors, one would expect a decrease in bond strength of an hydrogen atom bonded to a Ni atom if the number of Ni atom neighbors increases [33]. The very different result found derives from the strong asymmetry of the LDOS of the electron energy density in the face-centered cubic lattices discussed earlier (see Fig. 19) and depends strongly on band filling. At intermediate electron-band filling, increased delocalization dominates, but at the electron-band edges this inverts. This behavior can be completely understood from considerations based on the group orbital density of states at the Fermi level [33, 51]. Figure 27 shows the computed spectrum of Ni₂₀ and N₂₀H molecular orbitals. Note that hydrogen-type orbitals systematically shift to lower energy with increasing hydrogen-atom coordination number. These orbitals clearly are of the bonding type. Antibonding orbitals are

Table 5. Bond parameters for H binding sites [76]

Site	Description		Bond length (Å)		Vibrational frequency (meV)	Chemisorption energy (eV)
	Surface	Ligancy of H ^a	R _⊥ ^b	R _c ^c		
B	<001>	1(7)	1.50	1.50	283	1.56
F	<110>	1(5)	1.49	1.49	280	1.43
C	<112>	1(7)	1.49	1.49	(231)	(1.00)
A	<001>	2(7)	0.99	1.59	177	2.73
G	<001>	2(5)	0.99	1.59	(173)	(2.17)
E	<110>	2(6)	0.93	1.55	(161)	(1.56)
H	<112>	2(5)	0.96	1.57	176	2.43
I	<111>	3(5, 5) hcp	0.78	1.63	155	3.21
D	<111>	3(6, 7) fcc	0.79	1.64	(131)	(2.12)
J	<001>	4(7, 5)	0.30	1.78	73	3.04

^a In parentheses is the number of nearest neighbors for the Ni atom(s) binding site. Where nonequivalent surface atoms are present, values are given for each type

^b Optimum distance from H to the plane representing the surface

^c Distance from H to nearest neighbor Ni atoms

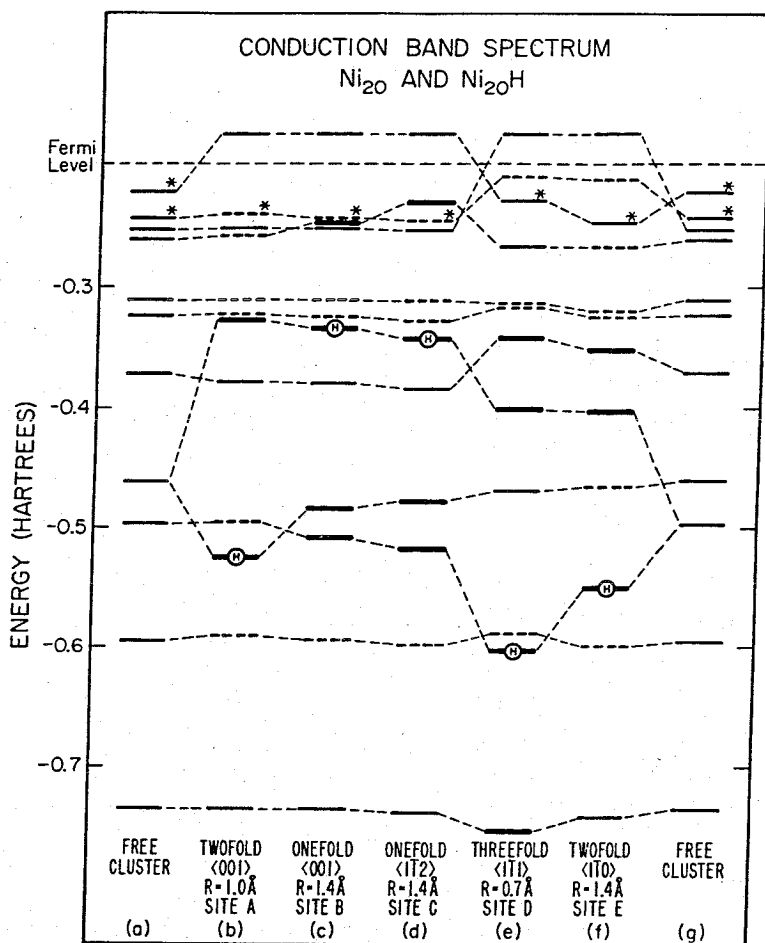


Fig. 27. Spectrum of states for Ni₂₀ and Ni₂₀H clusters. Levels connected by light dashed lines are of similar orbital character. Heavy lines indicate levels interacting significantly with the H atom. The H on a level indicates the orbital with maximum H character. Dashed levels are for orbitals unable to interact with the H atom by symmetry. Asterisks indicate simply occupied orbital levels. The d levels are spatially localized and have been replaced by an effective potential. The position of the Fermi level is approximate and is used primarily to distinguish between occupied and unoccupied levels [76]

shifted above the Fermi level (and become empty). According to Upton and Goddard, the bond strengths calculated correlate with the coefficients of the interacting atomic orbitals of molecular orbitals close to the Fermi level. In other words, there appears to be a relation with the local density of states of the group orbital at the Fermi level, as suggested by Eq. (28).

In summary, symmetry considerations based on frontier orbital theory enable a good understanding of H₂ dissociation on transition-metal clusters. For a single atom, electron promotion energy and hybridization are important variables. In diatomics, the relative position of d versus s electrons determines whether the bonding symmetric s orbital built from s-atomic orbitals is occupied. Occupation of this

orbital usually implies large repulsive effects. These can be decreased by promotion to empty d orbitals. In the molecule, this promotion energy is usually less than that of the free atom. The dissociation energy of H_2 and the activation energy for H_2 dissociation is also less than that of the free atom, because now the dissociated atoms can bond to different atoms. Dependent on whether the σ orbital is occupied or not, increasing the cluster size will change the repulsive interaction originating from the interaction with this orbital. In addition, antibonding σ^* surface orbitals become populated, which favors metal electron backdonation into antibonding empty adsorbate orbitals.

The ionization energies of the metal clusters may decrease sharply for metals with a filled d band (e.g., Cu) enhancing backdonation further. This will be discussed more extensively in the following section. If the particle size increases further, delocalization increases and the interaction with adsorbates tends to decrease.

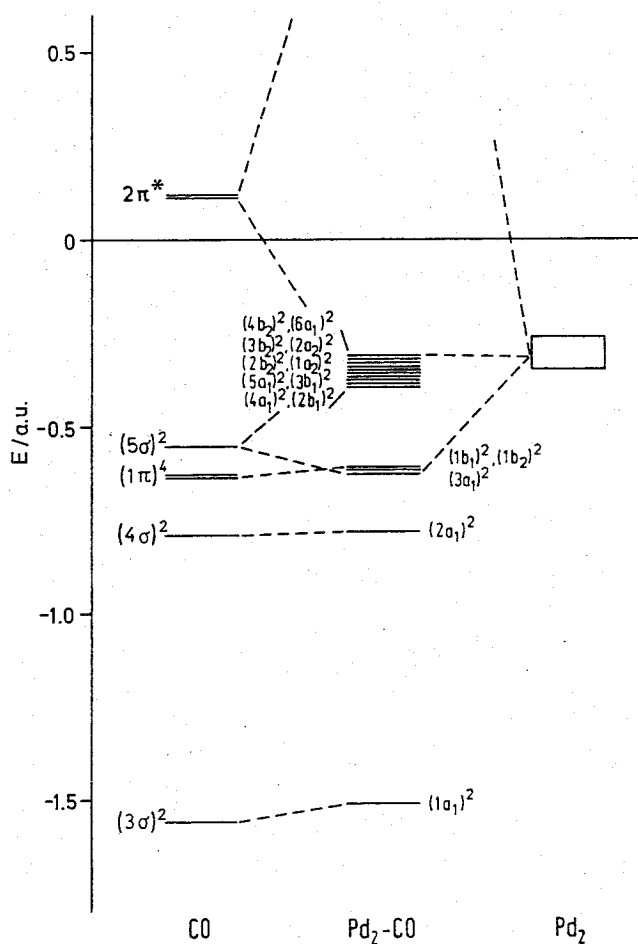


Fig. 28. Schematic MO diagram for the 1A_1 ground state of Pd_2-CO . The notation of the MOs in Pd_2-CO concerns the valence MOs only [77]

3.3 Cluster Chemisorption Models of CO Adsorption

Pacchioni and Koutecky [77] studied the interaction of CO with several Pd clusters using multireference doubly excited configuration interaction (MRD CI) procedures.

The schematic interaction scheme presented in Fig. 28 is very similar to that derived for the interaction with H_2 discussed earlier. The doubly occupied 5σ CO orbital interacts strongly with the empty symmetric σ orbital of Pd_2 consisting mainly of the Pd $5s$ atomic orbitals. This is a stabilizing interaction and electrons are donated to the metal.

The $2\pi^*$ level interacts with the occupied antisymmetric Pd atomic d orbital combination, resulting in a shift upwards for the CO $2\pi^*$ levels and a bonding stabilization of the Pd d-orbitals.

The bond strength increases from 6 kcal/mol for Pd-CO, and 13.2 kcal/mol for Pd_2CO , to 17.1 kcal/mol for Pd_3CO . So it increases with the number of metal neighbors of CO.

A recent study by Andzelm and Salahub [78] is available using the Local Spin Density method, with qualitatively similar results. Post and Baerends [79] studied chemisorption of CO to Cu clusters using the HFS- X_α method. Of interest to our discussion are their results for the interaction of CO with Cu_2 . In their calculation, CO approaches Cu_2 in a symmetrical way with its axis perpendicular to the Cu-Cu

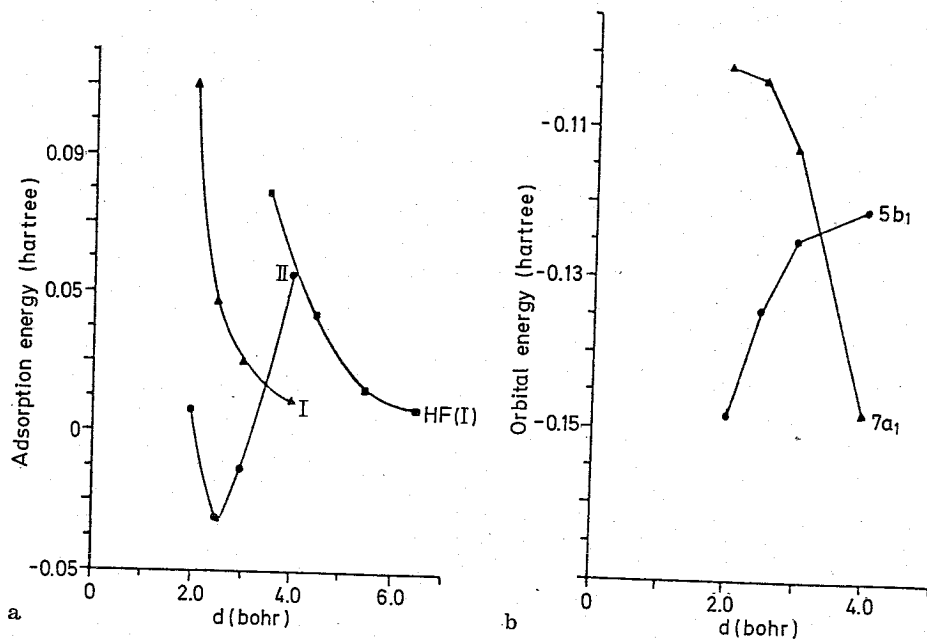


Fig. 29a. "Adsorption energy" as a function of the CO height above the band midpoint in Cu_2 for configurations I and II. The HF (Hartree-Fock) curve (for a Cu-Cu distance of 4.2 Bohr) is taken from: Kaleveld EW (1981) PhD thesis, University of Utrecht, The Netherlands; b. The Cu_2 ($4s + 4s$), CO $5\sigma(7a_1)$ and CO $2\pi^*(5b_1)$ one-electron energies as a function of CO height above the bridged position in Cu_2 [79]

axis. Since the Cu atom has one valence electron more than the Pd atom, the symmetric molecular orbital of Cu_2 built from the Cu 4s atomic orbitals is doubly occupied.

The HOMO of CO is its 5σ orbital. This orbital is also doubly occupied resulting in repulsive interaction with the Cu_2 σ orbital. This repulsion is not compensated by the electron backdonation interaction with the unoccupied CO $2\pi^*$ level (curve I, Fig. 29). Promotion of electrons from the Cu_2 $(4s+4s)\sigma$ to the empty Cu_2 $(4s-4s)\sigma^*$ molecular orbital, changes the repulsive interaction curve into an attractive one (curve II, Fig. 29a). A HOMO of σ^* symmetry becomes available for backdonation into the CO $2\pi^*$ orbital, and an unoccupied LUMO of σ symmetry becomes available to bonding with the doubly occupied 5σ CO orbital.

The most important effect of the configuration change from $(4s+4s)$ doubly occupied to $(4s-4s)$ doubly occupied is the disappearance of the 4-electron destabilizing interaction (exchange or Pauli repulsion) of the 5σ (carbon lone pair) orbital of CO with the $(4s+4s)$ metal orbital.

In particular, in large clusters such configuration changes almost always occur. The reason is that for an adsorbate like CO, with a pronounced lone pair orbital pointing toward the metal, the Pauli repulsion is large because of the large overlap of the lone pair orbital with metal orbitals. This point has also been stressed by Bagus et al. [30].

In a simple one-electron picture, the Pauli repulsion is due to the occupation of the destabilized antibonding orbitals (cf. Sect. 2).

In chemisorption to a metal, however, these antibonding orbitals will not remain occupied but they will become unoccupied as soon as they are "pushed" above the Fermi level. This corresponds to the configuration change in the metal cluster referred to above.

The implication is that the steric repulsion (caused by Pauli repulsion) calculated using the "frozen configuration" wave function Ψ^0 , introduced in Sect. 2a, is often relieved in the same way as in Cu_2 , by an electron transfer out of a repulsive σ orbital into a π orbital that can backdonate into the π^* of CO. The σ orbital that caused the repulsion with the CO 5σ due to a large overlap, will now for the same reason be a good acceptor orbital.

Therefore, large steric repulsion (or frozen orbital repulsion) does not imply that there will be no σ donation. It does, however, require a configuration change to make the σ donation possible.

We may clarify the situation by referring back to Fig. 5, which may serve to represent a number of interacting orbitals of σ symmetry. The Pauli repulsion corresponds to the destabilization of ψ_B , a typical substrate level close to the Fermi surface, and of χ_B , representing a manifold of levels well below E_F . As discussed in Sect. 2, the overlap region between ϕ_A and ψ_B and χ_B will be depleted of electron charge in Ψ^0 , with a concomitant lowering of the electrostatic energy and rise in kinetic energy.

Subsequently, there is the energy lowering from this situation to the converged wave function Ψ_{conv} , which arises from the orbital interactions of σ symmetry depicted in Fig. 5 and which may therefore be called σ bonding.

It consists of two types of electron rearrangement.

In the first place, the virtual orbitals will mix into the destabilized ψ_B and χ_B . This results in the more stable $\psi_{B'}$ and $\chi_{B'}$. In terms of electron rearrangements, this step consists of polarization and charge transfer.

In the second place, there is the depopulation of the $\psi_{B''}$ level if it remains above the Fermi level, in spite of the stabilization by the virtuals. It is, as often, somewhat hard to distinguish charge transfer and polarization in this last effect.

If B represents the metal (cluster), $\psi_{B''}$ will have predominantly metal character as will the level at the Fermi surface receiving the electrons. This means that this is mainly a rearrangement of electrons within the cluster, i.e., polarization of the metal.

As discussed earlier, one has to remember that the polarization discussed here is due to non-orthogonality of fragment orbitals and not due to the presence of an electrostatic field.

Still, the occurrence of polarization is at the same time an indication of some charge transfer. This is most clearly seen (see Ref [26]) when a configuration change is first achieved in the bare cluster so that ψ_B becomes empty, corresponding to the cluster polarization, and next the charge-transfer (HOMO-LUMO) type of interaction between φ_A and ψ_B is allowed to occur (σ donation).

A very interesting application and verification of these effects is provided in the work of Raatz and Salahub [80]. These authors studied the change in the magnetism of Ni upon chemisorption of CO. In agreement with the decrease of the saturation magnetization of transition-metal particles upon chemisorption found experimentally, they observe a decrease of the magnetic moments of the Ni atoms in their clusters near to the adsorption site.

The explanation is provided by the depletion of antibonding levels as discussed above. Part of the $d\sigma$ density of states is pushed above the Fermi level through antibonding interaction with CO (cf. ψ_B , resp., $\psi_{B''}$). This triggers a highly spin-dependent rearrangement of the d electrons. A 'hole' is created in the $d\sigma$ manifold which is compensated by an increased d density of states in other symmetries. As there are no majority-spin holes, the increase is in the minority-spin levels, leading to a reduction of the total net up-spin density. The authors noted that this magnetic effect is intimately related to the Ni-CO bonding, in the sense that the emptying of the antibonding levels relieves the Pauli repulsion which would otherwise result.

The effects discussed here are fairly large and will be found to occur at the SCF level in any reasonably accurate electronic structure method. It has, for instance, been shown by Baerends and Rozendaal [25] in a detailed study on $\text{Cr}(\text{CO})_6$ that the Hartree-Fock and X_α models yield completely analogous pictures of the importance of the various contributions (steric repulsion, σ bonding, π backbonding) to metal-carbonyl bonding.

Overall bonding is somewhat stronger in X_α than in Hartree-Fock owing to a stronger π bonding.

On the other hand, Bagus et al. [30] noted, upon comparing their Hartree-Fock results for CO interacting with an $\text{Al}_5(5, 0)$ cluster to previous X_α results for the same system obtained by Post and Baerends [41], that there was a huge discrepancy of ~ 5 eV in the calculated adsorption energies.

Whereas the X_α calculation resulted in a bonding energy of -1.9 eV for CO atop of the central Al atom of the $\text{Al}(5,0)$ cluster, at 3.7 Bohr distance, the Hartree-Fock calculation yielded an antibonding contribution by 2.5 eV at 3.5 Bohr, a difference of 4.4 eV.

Although X_α is known to give stronger bonding, this difference is too large to be attributed to a difference in the model (X_α or Hartree-Fock) used.

We have, therefore, repeated the Hartree-Fock calculations by Bagus et al. [30] using exactly the same Gaussian basis and the same geometry [81]. We do indeed reproduce the antibonding of 2.5 eV quoted in Ref [30], but only if we freeze in the $\text{Al}_5\text{-CO}$ system the electron configuration of the Al_5 part at the $(3a_1)^2 (1b_1)^2 (2e)^3$ ground state configuration of the bare Al_5 cluster. However, it had been noted in the X_α calculation that the highest occupied a_1 orbital of the Al_5 cluster ($3a_1$) has considerable $3p_z$ character on the central Al and, as a consequence, a sizable overlap with the CO 5σ orbital. As noted above for the $(4s + 4s)$ orbital of Cu_2 , and as has been found in many clusters [26], also in this case depopulation of the $3a_1$ orbital was found to occur as it was shifted above the Fermi level by the antibonding interaction with the Co 5σ orbital.

We have verified that precisely the same effect occurs in the Hartree-Fock calculation: changing the configuration to $(3a_1)^0 (1b_1)^2 (2e)^4 (1b_2)^1$ lowers the energy of the $\text{Al}_5\text{-CO}$ system by 3 eV. CO is, therefore, bound in Hartree-Fock to the Al_5 cluster by 0.5 eV. This is still considerably less than the 1.9 eV in the X_α calculation, but this difference is more in line with the usual difference between Hartree-Fock and X_α (or local density) calculations for CO interacting with metal clusters and for bond energies in general [83].

This example shows that it is incorrect to use unchanged cluster electronic configurations in chemisorption calculations. Most importantly, however, it shows that a gratifyingly similar picture of the importance of such effects as (relieve of) Pauli repulsion, configuration changes, polarization of the metal substrate, etc. emerge from such different electronic structure methods as Hartree-Fock and X_α (LSD).

Although the energy decompositions discussed so far provide a rather detailed understanding of the interaction of adsorbates with clusters, it remains an open question how accurately the cluster calculations mimic chemisorption. Among the many studies of the effect of cluster size, there are two on the Cu_n/CO system which used energy decomposition to consider the variation of the various energy contributions with cluster size and shape (Post and Baerends [26], and Hermann, Bagus, Nelin [84]).

The conclusions of these two studies are virtually identical. There are a number of properties of the CO/Cu system which converge fairly rapidly with cluster size, such as distance to the surface, vibration frequency, bond lengthening of CO, decrease of CO vibration frequency. The notable exception is the bonding energy of the adsorbate to the metal cluster, which shows strong variation with cluster size (cf. also Ref [78]).

Also the relative energies of different adsorption sites on clusters are different from those found on semi-infinite lattices, the hollow site, for instance, being strongly preferred in calculations for CO on Cu clusters, whereas at surfaces, CO is found to adsorb atop.

Therefore, we conclude this section with a short discussion of the most important differences of the clusters compared with extended systems.

It has been noted [26, 84] that the chemisorption energy obtained with a small cluster depends on the "accidental" position of the important frontier orbitals of $\sigma(A_1)$ and $\pi(E)$ symmetry.

If, for instance, the a_1 frontier orbital is empty, or so little below E_F that it becomes unoccupied, the cluster is a good σ acceptor.

On the other hand, if an a_1 orbital that strongly overlaps the CO 5σ orbital (or the adsorbate lone-pair orbital in general) remains occupied, the cluster is not a good σ acceptor and there is strong Pauli repulsion.

It is clear from the results in Refs [26, 84] that, in particular, this repulsive term, which is large, varies considerably between the clusters. The positions of the crucial levels in the clusters have been termed "accidental" as they are determined, in small clusters, by the shape and size of the clusters.

The same arguments apply, *mutatis mutandis*, to the bonding contributions. Concentrating on the cluster orbitals originating from the metal s atomic orbitals, we note that the antisymmetric combinations important for π bonding will be occupied or unoccupied depending on the shape of the cluster and of course on the electron count of the metal. For instance, triangular or larger clusters of one-electron s -metals (Cu, alkalis) populate such orbitals. As demonstrated in Ref [26], such clusters have a strong interaction with CO in high coordination sites, with significant back-donation into the $2\pi^*$ orbitals of CO.

In the next section it will be shown that these effects are much smaller on extended lattices because electrons become delocalized. The effective population of antisymmetric "group orbitals" present in the cluster mentioned above, becomes much smaller in an extended lattice. The π interaction is therefore smaller on the extended substrate. The reverse may also happen. In metals that have too low an electron count to populate antisymmetric combinations of s atomic orbitals in small clusters (the d orbitals will be populated instead), embedding in an extended metallic lattice will populate such antisymmetric group orbitals to some extent. We already discussed such a situation for the Ni_{13} cluster. In such cases, interaction with π -type orbitals will be enhanced in the extended lattice as compared to the small cluster.

As discussed in the theoretical intermezzo, repulsion due to interaction of doubly occupied orbitals is proportional to the number of neighbours.

Calculations by Hermann et al. [85] confirm this for the interaction of NH_3 with an Al_{10} cluster, assuming 3A_2 symmetry (promotion absent). Whereas an overall bonding interaction is found for ammonia in the atop site, a strong repulsion is found in the threefold position (Fig. 30).

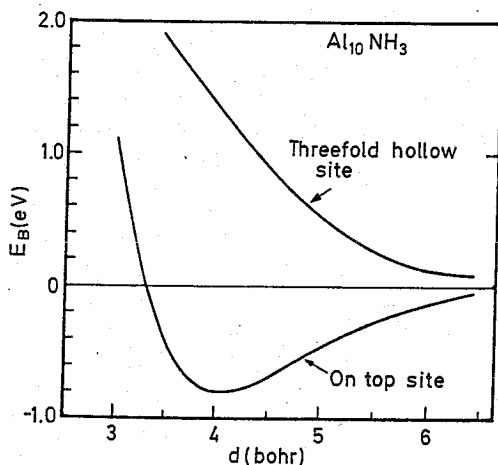


Fig. 30. Binding curves of the Al_{10} (7,3) NH_3 (on-top site), and the Al_{10} (3,7) NH_3 (threefold hollow site) clusters [85]

The more favorable backdonation into empty π -type orbitals of ammonium favoring the threefold position does not compensate for the strong repulsive effects experienced by the doubly occupied ammonia σ orbital in that position. This is understandable since the π acceptor orbitals of NH_3 are at very high energy. Even for CO, however, with low lying π acceptor levels, the topsite is preferred and the hollow site only weakly bonding [41].

4 Chemisorption to Metal Surfaces

General features of the chemical bond to a metal surface were described in Sect. 2.

Here, we will focus on those aspects of the surface chemical bond that sensitively depend on the distribution of the electrons over valence orbitals with a different angular distribution.

Studies of Hoffmann and Anderson [86, 87] as well as Baetzold [88] apply the extended Hückel method to the calculation of the electron distribution of molecules interacting with metal slabs.

We will use approximations to the extended Hückel method to derive a useful and convenient description of the local density of states of a metal. The methods developed in Sect. 2d are suitable to derive basic features of the surface chemical bond.

This is especially a suitable approach if one wishes to discuss the role of orbital symmetry in surface reactions.

Early work by Bond [89] and Weinberg and Merrill [90] used the orientation of d orbitals at a surface and Goodenough's [91] band theory to study the interaction of molecules and atoms with a surface.

A similar approach will be used here [37], but one based on more recent electron band models.

Trends will be discussed in the bond strengths and reactivities of CO and NO chemisorbed to different faces of group VIII transition metals with varying valence d electron count.

Of particular interest are the differences in coordination of CO to the surfaces of different metals.

At low surface coverage, CO adsorbs atop on the most dense faces of Pt [92], Rh [93], Co [94], and Cu [95], but it adsorbs in a bridge coordination on the (111) face of Ni [96].

We also intend to indicate the reasons for the differences in face dependence of the reactivity comparing different Pt faces to that of Rh.

Finally, the opposing trends in CO bond strength and H bond strength found for elements in the last row of group VIII metals will be explained [37].

The work-function dependence according to Eq. (28) results in similar effects of the electrostatic field on chemisorption as found from first-principle calculations [11], effective medium theory [10], or adapted extended Hückel theory [55].

Lowering the effective ionization potential enhances electron backdonation between metal and adsorbate. The authors have discussed this effect extensively elsewhere

[51]. Also earlier we discussed the use of Eq. (27) to interpret coadsorption effects [51].

The changes of the surface group-orbital local density of states at the Fermi level (see Sect. 2d for definition), computed in the presence of coadsorbates (e.g., S) [97] can be inserted into Eq. (28) to compute the resulting energy changes.

The following simplified model of the electronic structure of the transition-metal surface is very useful to discuss the elementary interactions playing a role in the formation of the surface-adsorbate chemical bond.

In the bulk, a f.c.c. metal atom has 12 nearest neighbors. As sketched in Fig. 31, the three d_{xy} , d_{yz} , d_{zx} , x orbitals each have 4 nearest neighbors which are not shared.

This leads to a symmetric electron density of states, threefold degenerate in the three perpendicular planes.

The d_{z^2} and $d_{x^2-y^2}$ orbitals have nearest neighbors at a $\sqrt{2}$ larger distance than the d_{xy} , d_{yz} and d_{zx} atomic orbitals. The d_{z^2} and $d_{x^2-y^2}$ orbitals will form a twofold degenerate electron band of much narrower bandwidth than the d_{xy} , d_{yz} , and d_{zx} orbitals.

Since the overlap between the s and p atomic orbitals is much larger than between the d atomic orbitals, they will form a broad band, usually overlapping the much smaller d valence-electron energy band.

This is sketched in Fig. 32 for the s and d bands.

For a f.c.c. crystal, the s valence-electron band is strongly asymmetric as discussed earlier [51], the d valence-electron bands are symmetric as long as only interactions between nearest neighbors are considered and the overlap matrix is assumed to be diagonal.

For group VIII metals, a good approximation gives 1 electron per atom in the s valence-electron band and varying electron number in the d valence-electron band.

Because the d valence-electron bands are nearly completely filled for the metals Ni, Pd, or Pt, one expects holes in the d valence-electron band to have considerable d_{xy} , d_{yz} , and d_{zx} and little d_{z^2} and $d_{x^2-y^2}$ character.

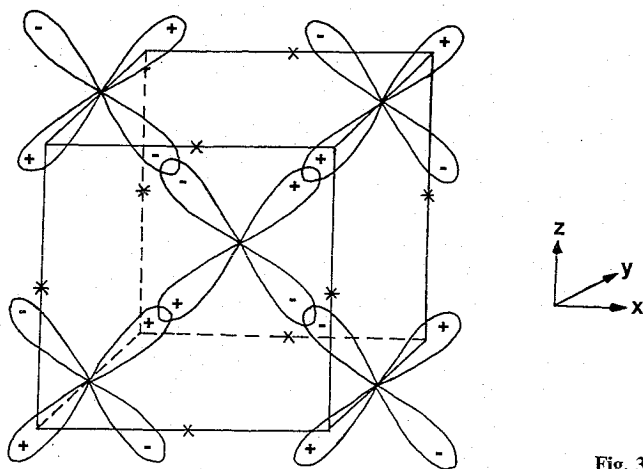


Fig. 31. d_{xy} orbitals in f.c.c. crystal

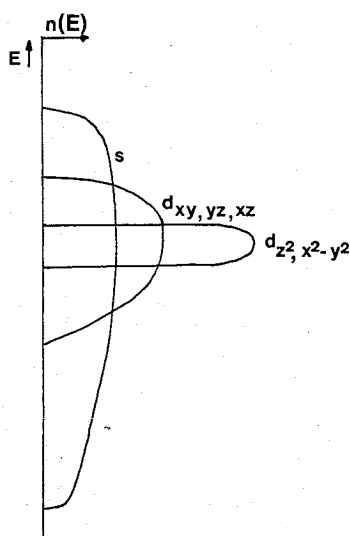


Fig. 32. Band structure (schematic) of f.c.c. metal [51]

The picture of the valence-electron structure presented is, of course, highly schematized; nonetheless, extended Hückel calculation on slabs indicate the general validity of the schematic electron distribution derived earlier [98]. In Fig. 33, 34, and 35, the respective changes at the (111), (100), and (110) surfaces of the d_{xy} , d_{yz} , and d_{zx} valence-electron bonds are sketched.

In the sense of the second-order perturbation theory expression for the energy, only those orbitals have to be considered, because for the group VIII metals in the last columns of the periodic system they are the only ones to have a finite density of states at E_F .

At the (111) surface, each of the d_{xy} , d_{yz} , and d_{zx} surface orbitals loses one neighbor. The resulting orbital configuration is sketched in Fig. 33 a.

As pointed out by Kahn and Salem [99], the three degenerate dangling surface orbitals will rehybridize according to the local symmetry of the surface atoms.

As a result, two degenerate asymmetric surface orbitals and one symmetric surface orbital is formed:

$$\phi_1^{as} = \frac{1}{\sqrt{2}} (\phi_{d_{xy}} - \phi_{d_{yz}}); \quad \phi_2^{as} = \frac{1}{\sqrt{6}} (\phi_{d_{xy}} + \phi_{d_{yz}} - 2\phi_{d_{zx}})$$

$$\phi_3^s = \frac{1}{\sqrt{3}} (\phi_{d_{xy}} + \phi_{d_{yz}} + \phi_{d_{zx}})$$

The original degeneracy is lifted by the presence of the metal surface and the resulting surface symmetry electron density of states is sketched in Fig. 33 c (the figure is the result of a Bethe lattice approximation calculation). It is essential to consider this lifting of degeneracy and the creation of asymmetric orbital combinations, since some authors, e.g., Banholzer et al. [100], have erroneously ignored this. As a result,

their relations between symmetry of surface orbitals and adsorbate are based on an incorrect use of surface orbital analysis.

As is seen in Fig. 33c, the maximum in LDOS of the asymmetric LDOS ($d\pi$) is at higher energy than that of the symmetric part ($d\sigma$). After hybridization, the surface orbitals can be represented as sketched in Fig. 33b.

Interaction between lobes originating from different surface atoms, but directed towards the missing atom, can also be considered and will lead to symmetric and asymmetric combination of atomic orbitals directed towards the threefold position.

At the (100) surface, the d_{yz} orbital in the (100) plane does not lose any neighbors.

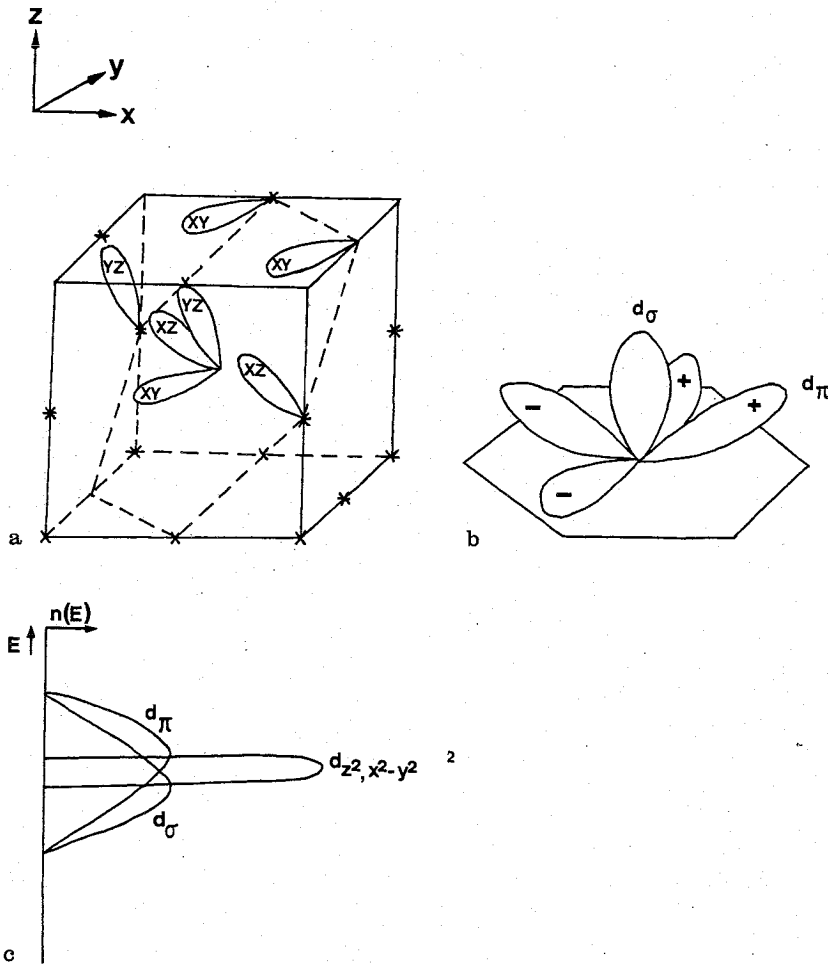


Fig. 33a-c. d-valence electron distribution at the (111) surface. a. The out-of-plane lobes of the degenerate d_{xy} , d_{yz} , and d_{zx} atomic orbitals [37]. b. The linear combinations of the plane lobes of the d_{xy} , d_{yz} , and d_{zx} atomic orbitals symmetry adapted to the (111) surface. c. Scheme of surface d-electron density of states

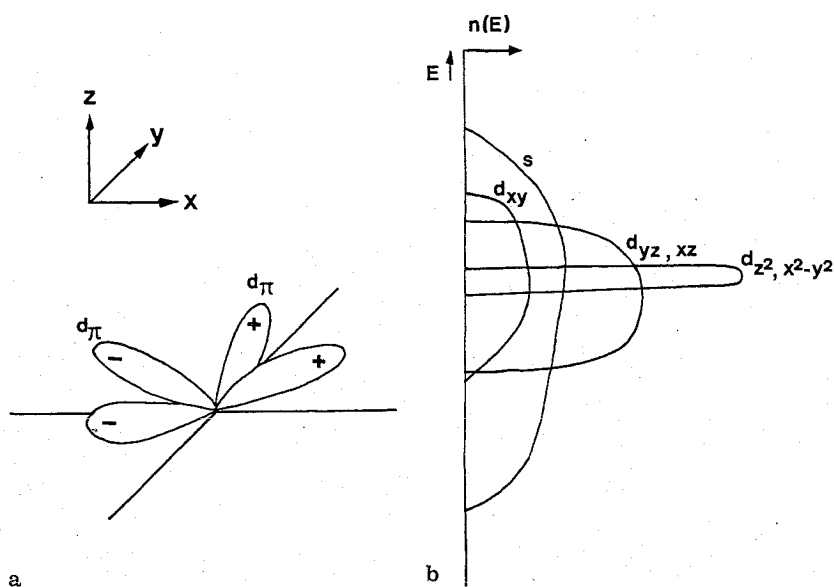


Fig. 34 a, b. d-valence electron distribution at the (100) surface, a. d_{xz} and d_{yz} lobes. b. Schematic sketch of surface electron density of states [37]

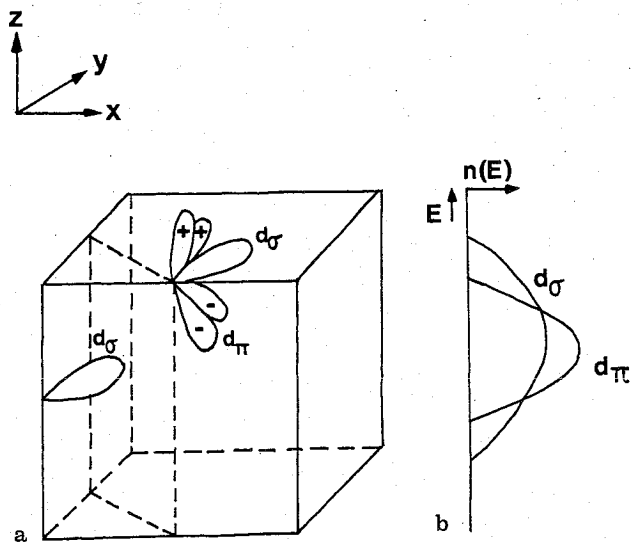


Fig. 35 a, b. d-valence electron distribution at the (110) surface, a. d_{xz} , d_{yz} , and d_{xx} lobes. b. Schematic d-valence electron density of states

The d_{xy} and d_{zx} orbitals each lose two neighbors. As a result, the local density of states $\rho_i(E)$ at the surface is split into two bands, a broad band corresponding to the d_{yz} orbitals and two more narrow bands d_{xy} , d_{zx} , with a higher electron occupation (see Fig. 34).

At the (110) surface, two different atoms are generated, atoms a and b (Fig. 35). Atom a loses one neighbor, resulting in a dangling orbital σ symmetric into the direction perpendicular to the surface.

The edge orbitals of t_{2g} symmetry are missing 5 neighboring orbitals. This generates one σ -dangling orbital and two π symmetry orbitals, as sketched in Fig. 35.

To summarize, at the (111) surface orbitals of σ as well as π symmetry are generated with a bandwidth corresponding to three neighbors, instead of four as in the bulk. At the (100) surface, only dangling bonds of π symmetry are generated, with a smaller bandwidth corresponding to two neighbors.

The edge atoms of the (110) surface have one σ and two π -type dangling bonds. The σ dangling bond has a broader bandwidth than the π -type bond.

Let us first discuss the consequences of this orbital scheme for the interaction with an orbital of σ symmetry (H atoms, 5σ orbital of CO, etc.).

In the atop adsorbed state, a σ -type orbital will only interact with the (111) and (110) surface d orbitals, because at the (100) face no d orbital of σ symmetry with a finite density of state at the Fermi level is available.

In this approximation the contribution of the interacting d_{z^2} and $d_{x^2-y^2}$ orbitals that are doubly occupied, but positioned below E_F is ignored.

Since the σ -dangling bond bandwidth at the (111) face and (110) face is comparable, the interaction will be the same.

So, a σ adsorbate orbital with one electron in its orbital will bind with comparable energy to the (111) as well as (110) d orbitals in the atop configuration. There will be no interaction with the d orbitals at the (100) face.

A σ orbital with two electrons in its orbital will have a repulsive interaction with other doubly occupied orbitals.

At the end of the group VIII transition-metal series, the d orbitals contain a total of 9 electrons, this results in a 5/6 orbital occupation of the d_{xy} , d_{yz} , and d_{zx} orbital bands.

The orbital occupation of the σ -type dangling bond will be even higher because of its narrower surface bandwidth. As a result, the LDOS $\rho_i(E)$ at the Fermi level will be low, resulting in an overall repulsive interaction between a doubly occupied adsorbate σ orbital and the (111) as well as (110) surface σ dangling d lobe. Clearly, these repulsive effects may be converted into attractive effects if the σ dangling orbitals become depleted of electrons, as is the case for elements in the left column of the group VIII transition metals. For instance, for Rh and Co, the bulk orbital occupancy of the d_{xy} , d_{yz} , and d_{zx} orbitals is 1/2, resulting in a significant increase in the LDOS $\rho_i(E)$ at E_F for those metals. This decreases the repulsive interaction with doubly occupied σ orbitals significantly or converts it to an attractive one.

π -Type d surface orbitals interact with π -type adsorbate orbitals on all three surfaces. Since the bandwidth of the π -type d orbitals at the (110) and (100) surfaces are smaller than at the (111) face, one may expect at intermediate d-electron occupation a higher LDOS and electron occupation for those orbitals at the (110) or (100) surfaces than the (111) face.

So one expects on Pt, with a nearly completely filled d-valence electron band that adsorbed molecules such as NO and CO in the atop position favor binding to the (100) face, since then repulsion with the adsorbate orbitals is minimized and the attractive contribution dominates.

Clearly, this will be only the case if interaction with the d valence electrons dominates, since because of symmetry the adsorbate π electrons do not interact with the s valence-band electrons in this position.

In bridging or higher coordinated positions the π adsorbate orbitals will interact with antisymmetric combinations of surface metal s orbitals, hence this interaction with π adsorbate orbitals tends to favor bridge coordination.

Thus, the bonding interaction with the d valence electrons increases if the d occupancy decreases from 9 to 8 electrons. The d valence-electron occupancy then shifts to the center of d valence bands, where the LDOS at the E_F is maximum.

On Pt, CO adsorbs atop, but on Ni, CO adsorbs in bridging coordination. The work function of Pt is larger than that of Ni, 5.65 and 5.15 (eV) [100], respectively, so that the contribution of $2\pi^*$ donation is least on the Pt surface.

As discussed in Sect. 2, the 5σ orbital of CO has the largest attractive interaction with the s valence electrons in the atop position, since the LDOS at the E_F is highest in that position.

The interaction between the 5σ electrons and the σ d valence dangling-bond electrons is repulsive. The repulsive effect is proportional to the number of neighbors, this favors also atop adsorption.

It has been found for NO, that it dissociates more rapidly on the 100 surface than on the (111) and (110) surfaces of Pt [100].

On all three surfaces, there is a favorable interaction of π symmetry. As discussed, the repulsive interaction with the σ orbitals will be least at the (100) surface. Comparing π symmetric interactions, they will be favored on the (100) surface compared to the (110) surface because of the higher degree of coordinative unsaturation at the (110) face.

This may explain the results of Nieuwenhuis et al. [101] for Rh, with one electron less than Pt, showing that the (110) face becomes more reactive with respect to the (100) surface than was the case for Pt.

The interaction of CO with Ni, Pd, and Pt increases from Ni to Pt. This indicates also an increasing contribution of the adsorbate to metal donation interaction to chemical bonding and domination of the σ donating term over the $2\pi^*$ backdonating term. The increasing repulsive interaction with the d valence electrons tends to favor also the atop position for CO adsorbed to Pt.

Because of the decrease in work function, $2\pi^*$ backdonation increases from Pt to Ni. This is reflected in the favored bridge-coordinated adsorption site of CO to Ni and Pd.

In contrast to CO, the bond strength of hydrogen atoms increase from Pt to Ni. Whereas bonding in the hydride molecule is larger in PtH than in NiH, at the surface bonding to Ni is stronger [37]. Part of this change in sequence is due to prehybridization of Ni at the Ni metal surface compared to that of the Ni atom (bonding to the Ni atom requires electron promotion).

The same holds, of course, for Pd.

The orbital occupancy of the hydrogen atoms is half. The work function decrease from Pt to Pd to Ni will favor bonding to the Ni surface if electron backdonation dominates chemical bonding.

As demonstrated in the discussion on oxidative addition, the metal hydride bond gives an excess negative charge on the adsorbed H atom.

Comparing the bond strength in the M-H molecule and that of an H atom to the metal surface, one finds that bonding of the metal surface of Pt is significantly decreased [37]. This reflects the importance of the electron localization term in the energy to the bond strength of the adsorbate metal surface bond [33, 37].

The *localization* energy of an electron is the energy required to decouple a metal electron from the metal lattice valence-electron band and localize it on a surface atom, so that it can bind to an adsorbate. If a metal valence electron band is half filled, this will result in a decrease of the metal adsorbate bond strength. The localization energy is not present in a single metal atom, where, on the other hand, the electron promotion energy is an important energy term.

As discussed, CO chemisorption to Pt in the atop position is ascribed to the dominance of the interaction with CO 5σ electrons.

On Ir, Rh, and Co the depletion of the d valence-electron band enhances the local density of states of the d electrons at the Fermi level, and it appears that the interaction with the doubly occupied σ orbitals may become attractive. Whereas on the Ni surface backdonation into the $2\pi^*$ orbitals is favored over σ donation and, as a consequence, bridge adsorption is favored, on Co the increased interaction with the d valence electrons enhances the $2\pi^*$ backdonation in the atop position with respect to the bridge position, changing the balance to the atop position. The same happens on Rh compared to Pd.

On Pt, the high work function decreasing backdonation into the $2\pi^*$ orbitals and the spatial extension of the d orbitals resulting in a large repulsion help to favor the atop configuration.

On Ir, the interaction with the d band will be significantly enhanced and some increase in $2\pi^*$ backdonation is expected. Again the atop position is expected to be favored.

Comparing Cu with Ni, the attractive part of the bond energy should become more dominated by $2\pi^*$ backdonation, because of the further decreased work function.

The total bond strength, however, decreases because of the loss of d valence-electron density at the Fermi level.

All of the d valence-electron orbitals now are doubly occupied and their interaction with the 5σ orbitals becomes exclusively repulsive. Since repulsive effects are lowest for minimum coordination, atop adsorption results [31].

We will conclude this section with a short discussion of the effect of explicitly including orbital overlap on the LDOS $\rho_i(E)$ of adsorbate orbitals. Figure 36 [31] compares the LDOS of the CO 5σ and $2\pi^*$ orbitals of CO chemisorbed on Pt, as well as the computed metal valence d and s surface local density of states.

These are results of Bethe lattice approximation to the extended Hückel method calculations

One observes very clearly the earlier-discussed loss of electron density in the bonding

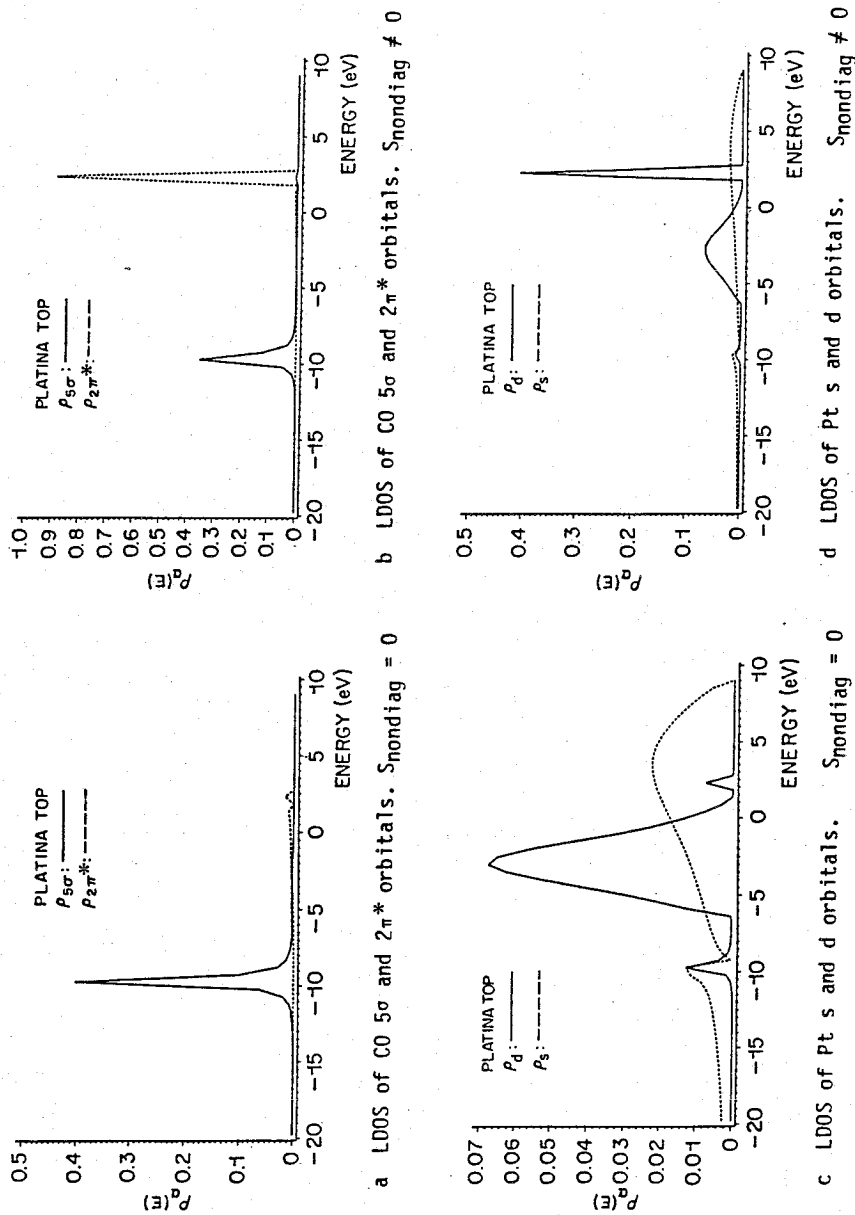


Fig. 36a-d. Local density of states for $S_{\text{nonbonding}} = 0$ and $S_{\text{nonbonding}} \neq 0$; CO chemisorbed atop of Pt. Bethe lattice approximation [31].

a. LDOS of CO 5σ and 2π* orbitals. $S_{\text{nonbonding}} = 0$
b. LDOS of CO 5σ and 2π* orbitals. $S_{\text{nonbonding}} \neq 0$
c. LDOS of Pt s and d orbitals. $S_{\text{nonbonding}} = 0$
d. LDOS of Pt s and d orbitals. $S_{\text{nonbonding}} \neq 0$

region and the increase of electron density in the antibonding region if the overlap matrix is assumed to be nondiagonal.

This is completely in line with the electron polarization effects discussed earlier due to non-orthogonality of the interaction fragment orbitals.

5 Summary

This review of chemical bonding to metal surfaces again demonstrates the power of symmetry concepts to predict changes in chemical bonding.

On small metal particles, classical notions of electron promotion and hybridization are found to apply.

In large particles and metal surfaces, prehybridized atoms occur, but now localization of electrons on the atoms involved in the metal surface bond becomes necessary.

Whereas in small particles the electrons are distributed over discrete energy levels, at a metal surface this electron distribution becomes continuous. Bonding between small particles and adsorbing molecules can be discussed in terms of the formation of bonding and antibonding orbitals.

Bonding of molecules to a semi-infinite lattice also leads to changed electron distributions that can be interpreted in terms of bonding and antibonding contributions.

This becomes in particular apparent if one studies the electron bond order density distributions.

If the interaction between adsorbate and metal electrons is small compared to the bandwidth of the metal electron valence band, interaction leads to broadening of the surface electron distributions.

The bond energy does not relate to the bandwidths of the broadened levels, but to the group orbital local density of states at the Fermi level projected out from the surface eigenfunctions by the adsorbate orbitals.

6 List of Symbols

HOMO	Highest occupied molecular orbital
LUMO	Lowest unoccupied molecular orbital
Ψ	State wave function
$\phi, \chi, \psi, \varphi$	One electron wave functions
\hat{A}	Antisymmetrization operator
$\rho_{i,i}$	Local density of states of orbital i
S	Overlap
$P_{\mu,\nu}$	Bond order
$\rho_{\mu,\nu}$	Bond order density
$F_{\mu\nu}$	Fock matrix
H	Hamiltonian operator
T	Kinetic energy operator
Z_A	Nuclear charge of atom A

$E_{(\text{exch}, s)}$	Electron exchange potential
$\Delta_{x, \text{REP}}$	Exchange repulsion energy
c_i^k	Coefficient of atomic orbitals i in molecular orbital k
u_i^k	Normalized coefficients of atomic orbitals in molecular orbital k
α_i	One electron energy of atomic orbital i
β_{ij}	Overlap energy between atomic orbitals i and j
Δ	Dispersion energy
Z	Number of atom neighbors
E_i	Molecular orbital eigenvalue
$\Delta n(E)$	Change in number of electrons of energy E
q_i	Charge on atom i
$G_{\nu, \nu'}$	Green's function
$\Gamma(E)$	Linewidth function
$A(E)$	Lineshift function
P_α	Orbital occupation fraction of electron band α
Δ_α	Bandwidth of electron band α
E_F	Fermi level
k_d	Screening length of orbital
σ	Symmetric orbital
σ^*	Antisymmetric orbital
π	Symmetric p-type orbital
π^*	Antisymmetric p-type orbital
ϕ	Angle

7 References

1. Woodward RB, Hoffman R (1961) *Ang Chem Int Ed Engl* 8: 781; Hoffman R (1982) *Ang Chem Int Ed Engl Science* 21: 711
2. Fukui K (1982) *Science* 218: 747
3. Pearson RG (1971) *Acc Chem Res* 4: 152
4. van der Avoird A, Wormer PES, Mulder F, Berns RM (1986) *Top Curr Chem* 93: 1
5. March NH (1986) *Chemical Bonds outside metal surfaces*, Plenum
6. van Santen RA (1985) *J Chem Phys* 83: 6039
7. Grunze M, Kreuzer HJ (eds) (1986) *Kinetics of Interface Reactions*, Springer Series in Surface Sciences, vol. 8 Springer, Heidelberg—Berlin—New York
8. Campbell CT (1986) *Surf Sci Lett* 173: 641
9. Geerlings JJC, Los J (1984) *Phys Lett A* 102: 204
10. Norskov JK, Holloway S, Lang ND (1984) *Surf Sci* 137: 65
11. Wimmer E, Fu CL, Freeman AJ (1985) *Phys Rev Lett* 55: 2618
12. Backx C, de Groot CPM, Biloen P (1981) *Surf Sci* 104: 300
13. Barteau MA, Madix RJ (1980) *Surf Sci* 97: 101
14. Norskov JK, Besenbacher F (1987) *J Less Common Metals* 130: 475
15. Kitaura K, Morokuma K (1976) *Int. J Quantum Chem* 10: 325
16. Morokuma K (1977) *Acc Chem Res* 10: 244
17. Kitaura K, Sakaki S, Morokuma K (1981) *Inorg Chem* 20: 2292
18. Wolfe S, Mitchell DJ, Whangbo MH (1978) *J Am Chem Soc* 100: 1936
19. Bernardi F, Bottoni A, Mangini A, Tonachini G (1981) *J Molec Struct (Theochem)* 86: 163
20. Stone AJ, Erskine RW (1980) *J Am Chem Soc* 102: 7185
21. Noell JO, Morokuma K (1979) *Inorg Chem* 18: 2774

22. Ziegler T (1985) *Inorg Chem* 24: 1547
23. Ziegler T, Tschinke V, Becke A (1987) *J Am Chem Soc* 109: 1351
24. Bauschlicher CW, Bagus PS (1984) *J Chem Phys* 81: 5889
25. Baerends EJ, Rozendaal A (1986) in: Veillard A (ed) *Quantum Chemistry: The Challenge of Transition Metals and Coordination Chemistry*, Nato, ASI series, Reidel, Dordrecht, p 159
26. Post D, Baerends EJ (1983) *J Chem Phys* 78: 5663
27. Bauschlicher Jr. CW, Bagus PS, Nelin CJ, Roos BO (1986) *J Chem Phys* 85(1): 354
28. Bagus PS, Hermann K, Bauschlicher CW (1984) *J Chem Phys* 80: 4378
29. Hermann K, Bagus PS, Nerlin CJ (1987) *Phys Rev B* 35: 9467
30. Bagus PS, Nerlin CJ, Bauschlicher CW (1983) *Phys Rev B* 28: 5423
31. Norskov JK, Lang ND (1980) *Phys Rev B* 21: 2131
31. van Santen RA (1988) *J Mol Struct* 173: 157
32. Pauling L (1931) *J Am Soc* 53: 1367; see also Coulson A (1961) *Valence*, Oxford University Press
33. van Santen RA (1987) *Progr Surf Sci* 25: 253
34. Newns PM (1969) *Phys Rev* 178: 1123
35. Grimley TB, Torrini M (1973) *J Phys C* 6: 868
36. Schrieffer JR (1972) *J Vac Sci Techn* 9: 561; Einstein TL, Schrieffer JR (1973) *Phys Rev B* 7: 3627
37. van Santen RA (1982) *Recl Trav Chem Pays-Bas* 101: 121
38. van den Hoek PJ, Tenner AD, Kleyn AW, Baerends EJ (1986) *Phys Rev B* 34: 5030
39. Feinberg MJ, Ruedenberg K (1971) *J Chem Phys* 54: 1495
40. Fujimoto H, Osamura J, Minato T (1978) *J Am Chem Soc* 100: 2954
41. Post D, Baerends EJ (1982) *Surf Sci* 116: 177
42. Bauschlicher CW (1986) *Chem Phys* 106: 391
43. Ziegler T, Rauk A (1977) *Theoret Chim Acta* 46: 1
44. Hoffmann R (1963) *J Chem Phys* 39: 1397; Hoffmann R, Lipscomb WN (1962) *J Chem Phys* 36: 2179; Hoffmann R, Lipscomb WN (1962) *J Chem Phys* 37: 2872; Albright ThA, Burdett JR, Whangbo MH (1985) *Orbital Interactions in Chemistry*, Wiley, New York
45. Anderson AB (1975) *J Chem Phys* 62: 1187
46. van Santen RA (1979) *J Chem Phys* 71(1): 163
47. Koutecky J (1958) *Trans Far Soc* 54: 1038; Koutecky J (1957) *Phys Rev* 108: 13
48. Grimley TB, Pisani C (1974) *J Phys C* 7: 2831; Pisani C (1978) *Phys Rev B* 17: 3134
49. Schrieffer JR (1974) in: *Dynamic Aspects of Surface Physics*, Goddman FO (ed) *Proc Int School of Physics "Enrico Fermi", Course XVII*
50. van Santen RA, Toneman LH (1977) *Int J Quantum Chem* 12, suppl 2: 83
51. van Santen RA (1987) *J Chem Soc Far Trans* 1, 83: 1915
52. Callaway J (1971) *Phys Rev B* 3: 2556
53. Seel M, Del Re G, Ladik J (1982) *J Comp Chem* 3: 451
54. Haydock R, Heine V, Kelly MG (1975) *J Phys C: Solid State Phys* 8: 259
55. van Santen RA (1984) *Proc 8th Int Catal Conf Berlin*, pp 97; Dechema: *J Phys C, Solid State Phys* (1982) 15: L513
56. Khanra BC (1983) *Chem Phys Lett* 96: 76
57. Grimley TB (1976) *CRC Crit Rev in Solid State Sci*, pp 239
58. Wang CS, Freeman AJ (1979) *Phys Rev B* 19: 4930
59. Kelly MG (1974) *Surf Sci* 43: 587
57. Grimley TB (1976) *CRC Crit Rev in Solid State Sci*, pp 239
58. Wang CS, Freeman AJ (1979) *Phys Rev B* 19: 4930
59. Kelly MG (1974) *Surf Sci* 43: 587
60. Gadzuk GW (1976) *NATO Adv Study Inst Ser, Phys Ser B*, vol 16, Plenum, NY
61. Salem L, Elliott R (1983) *J Mol Structure* 93: 75
62. Grimley TB (1986) *Phil Trans Roy Soc (London)* A318: 135
63. Shustorovich E (1982) *Solid State Comm* 44: 567; Shustorovich E, Baetzold RC, Muettterties EL (1983) *J Phys Chem* 87: 1100; Shustorovich E (1984) *J Phys Chem* 88: 1927
64. Blomberg MRA, Siegbahn PEM (1983) *J Chem Phys* 78: 5689
65. Brandemark UB, Blomberg MRA, Petterson LGM, Siegbahn PEM (1984) *J Phys Chem* 88: 4617
66. Low JJ, Goddard WA (1984) *J Am Chem Soc* 106: 6928
67. Low JJ, Goddard WA (1984) *J Am Chem Soc* 106: 8321

68. Nakatsuji H, Hada M, Yonezawa T (1987) *J Am Chem Soc* 109: 1902
69. Kitaura K, Obara S, Morokuma K (1981) *J Am Chem Soc* 103: 2891
70. Noell JO, Hay PJ (1984) *J Am Chem Soc* 106: 6928
71. Dedieu A (1985) in: Gielen M (ed) *Topics in Organometallic Chemistry*, Vol. 1, pp 1, Freund Publishing House, London
72. Berke H, Hoffmann R (1978) *J Am Chem Soc* 100: 7224
73. Zheng Ch, Hoffmann R (1988) *J Am Chem Soc* 110: 749
74. Melius CF, Moskowitz JW, Mortola AP, Baillie MB, Ratner MA (1976) *Surf Sci* 59: 279
75. Siegbahn PEM, Blomberg MRA, Bauschlicher Jr, CW (1984) *J Chem Phys*, 81(4): 2103
76. Upton ThH, Goddard WA (1981) *CRC Crit Rev in Solid State and Mat Sci*, pp 261
77. Pachioni G, Koutecky J (1987) *J Chem Phys* 78(9): 5663
78. Andzelm MJ, Salahub DR (1986) *Int J Quantum Chem* 29: 1091
79. Post D, Baerends EJ (1983) *J Chem Phys* 78(9): 5663
80. Raatz F, Salahub DR (1986) *Surf Sci* 176: 219
81. Baerends EJ, Siebbeles L, unpublished
82. Koutecky J, Hanke U, Fantucci P, Bonacic-Koutecky V, Papierouska-Kamienski D (1986) *Surf Sci* 165: 161
83. Painter GS, Averill FW (1987) *B35*: 7713
84. Hermann K, Bagus PS, Nelin C (1987) *Phys Rev B35*: 9467
85. Hermann K, Bagus PS, Bauschlicher CW (1985) *Phys Rev B31*: 6371
86. Sung S, Hoffmann R (1984) *J Am Chem Soc* 107: 2006; Sung S, Hoffmann R, Thiel P (1986) *J Phys Chem* 90: 1380; Hoffmann R, Zeng C (1982) in: Veillard (ed) *Quantum chemistry: The challenge of transition metals and coordination chemistry*, Nato, ASI series, Reidel, Dordrecht
87. Ray NK, Anderson AB (1982) *Surf Sci* 119: 35; Ray NK, Anderson (1983) *Surf Sci* 125: 803; Anderson AB, Awad MK (1985) *J Am Chem Soc* 107: 7854; Mechandru SP, Anderson AB, Ross PN (1986) *J Catal* 100: 210; Mechandru SP, Anderson AB (1986) *Surf Sci* 169: L281; Anderson AB, Grime RW, Hory SP (1987) *J Phys Chem* 91: 4245
88. Baetzold RJ (1983) *J Am Chem Soc* 105: 4271
89. Bond GC (1966) *Disc Far Soc* 41: 200
90. Weinberg WH, Merrill RP (1975) *J Catal* 40: 268
91. Goodenough JB (1963) *Magnetism and the chemical bond*, J Wiley, NY
92. Freitsheim H, Ibach H, Lehwald S (1977) *Appl Phys* 13: 147; Baro AM, Ibach H (1979) *J Chem Phys* 71: 4812
93. Dubois LH, Somorjai GA (1980) *Surf Sci* 91: 514
94. Backx C, unpublished
95. Hollins P, Pritchard J (1985) *Progr Surf Sci* 19: 275
96. Anderson S (1976) *Solid State Comm* 20: 229; Erley W, Wagner H, Ibach H (1979) *Surf Sci* 80: 612
97. Maclaren JM, Pendry JB, Joyner RW, Mehan P (1986) *Surf Sci* 175: 263; Maclaren JM, Pendry JB, Joyner RW (1986) *Surf Sci* L80: 165
98. Fassaert DJM, Verbeek H, van de Avoird A (1972) *Surf Sci* 9: 501
99. Kahn O, Salem L (1977) in: *Proc of the 6th International Congress on Catalysis*, London, 1: 101 (The Chemical Society, London)
100. Banholzer WF, Park PO, Mak KM, Masel RI (1983) *Surf Sci* 128: 176; Park PO, Banholzer WF, Masel RI (1983) *Surf Sci* 19: 145; Park PO, Banholzer WF, Masel RI (1985) *Surf Sci* 155: 341 and 653
101. Hendrickx HACM, Jongenelis APJM, Nieuwenhuys BE (1985) *Surf Sci* 154: 503; Hendrickx HACM, Nieuwenhuys BE (1986) *Surf Sci* 175: 185